Journal for ImmunoTherapy of Cancer

CD155 links tumor immunotype to epithelial-directed precision therapy beyond checkpoint inhibition in cervical cancer

Yannick Verhoeven ,[1,2] Delphine Quatannens,[1] Sanne van der Heijden,[1] Jari Claes,[3] Julie de Beukelaar,[1] Hilde Lambrechts,[1] Christophe Hermans,[1] Glenn Broeckx,[1,4] Herwig Van Dijck,[5] Ali Ramadhan,[5] Karen Zwaenepoel,[1,5] Hans Stoop,[5] Steven Van Laere,[1] Jan Hauspy,[6] Christel Faes,[3] Léon C van Kempen,[1,5] Xuan Bich Trinh,[1,2,7] Filip Lardon,[1] Senada Koljenovic,[1,5] Peter André van Dam,[1,2,7] Jorrit De Waele[1]

To cite: Verhoeven Y, Quatannens D, van der Heijden S, *et al*. CD155 links tumor immunotype to epithelial-directed precision therapy beyond checkpoint inhibition in cervical cancer. *Journal for ImmunoTherapy of Cancer* 2026;**14**:e014834. doi:10.1136/jitc-2026-014834

► Additional supplemental material is published online only. To view, please visit the journal online (https://doi.org/10.1136/jitc-2026-014834).

Accepted 05 May 2026

For numbered affiliations see end of article.

Correspondence to
Dr Jorrit De Waele;
jorrit.dewaele@uantwerp.be

ABSTRACT

Background Despite its viral etiology and immunogenic features, cervical cancer shows limited and often short-lived benefit from programmed cell death protein 1 blockade, currently the only approved immunotherapy for this disease. This limitation highlights the need for a deeper understanding of its immune microenvironment to uncover alternative or complementary immunotherapeutic targets that may improve outcomes.

Methods We integrated spatial proteomic and bulk transcriptomic profiling of the cervical cancer immune landscape. Immune subset markers (CD8, CD4, CD68, FoxP3, NKp46) and clinically actionable immune checkpoint molecules (HLA-E, CD47, CD73, CD276, CD155, Gal-9, PD-L1, CD70, LAG-3) were assessed by immunohistochemistry in 65 resected tumors, spatially resolved across tumor stroma and tumor epithelium niches. Expression patterns and correlations with clinicopathological variables, immunotypes, and survival were systematically analyzed. Key findings were cross-validated in The Cancer Genome Atlas cohort, and tumor-killing assays were conducted to evaluate the therapeutic potential of identified checkpoint axes.

Results Immune infiltration was predominantly localized to the tumor stroma, with $CD8^+$ and $CD4^+$ T cells as dominant subsets. Within the tumor epithelium, $CD8^+$ T cells and $CD68^+$ macrophages were most abundant. Among checkpoints, HLA-E and CD47 showed the highest and most widespread expression, whereas CD276 and CD155 were enriched in the tumor epithelium, and CD73 and CD70 in the tumor stroma. Squamous cell carcinoma showed a stronger immunologic profile than adenocarcinoma. Immunotype stratification revealed distinct expression profiles and prognostic patterns. Elevated niche-defined expression of CD8, CD4, CD4-FoxP3, and NKp46 associated with improved survival. CD155 emerged as the only checkpoint consistently linked with poor survival across niches and cohorts, and associated with chemotherapy resistance. Notably, CD155 was the most promising functional target and was highly and selectively enriched in the tumor epithelium across

WHAT IS ALREADY KNOWN ON THIS TOPIC

⇒ Cervical cancer is considered immunogenic due to its viral etiology, high mutational burden, and dense immune infiltration; however, responses to current immunotherapy remain limited. Programmed cell death protein 1 (PD-1) targeting therapy is the only approved strategy in this setting, yet its clinical efficacy is modest and alternative immunoregulatory pathways remain underexplored.

WHAT THIS STUDY ADDS

⇒ This study delivers an integrative spatial and transcriptomic immune landscape of cervical cancer, revealing that several alternative immune checkpoints are more consistently and abundantly expressed than programmed death-ligand 1. CD155 emerged as a reproducible prognostic marker across tumor niches and cohorts, and mechanistically demonstrated the strongest therapeutic potential among tested targets. Its consistent and near-exclusive enrichment in the tumor epithelium across all immunotypes, including immune-desert tumors, highlights its dual potential as a checkpoint molecule and a candidate for epithelial-targeted therapies, offering a novel and underrecognized therapeutic angle for precision therapy in cervical cancer.

HOW THIS STUDY MIGHT AFFECT RESEARCH, PRACTICE OR POLICY

⇒ These findings support moving beyond PD-1 blockade in cervical cancer and shift the perspective on targeting CD155, from conventional checkpoint inhibition towards precision immunotherapy guided by tumor architecture and immune contexture. This study may therefore provide a rational framework for the development and deployment of immunotype-guided, next-generation CD155-targeted therapies, such as antibody-drug conjugates, oncolytic viruses, bispecific T cell engagers, and chimeric antigen receptor-based cell therapies.

all immunotypes, including immune-desert tumors where other immune markers were scarce.

Conclusion This study reveals a complex, niche-specific and immunotype-specific immunoregulatory architecture in cervical cancer that extends well beyond programmed death-ligand 1. CD155 stands out as a compelling and underused therapeutic target, supporting a paradigm shift in targeting the T cell immunoreceptor with Ig and ITIM domains (TIGIT) axis. Its functional impact and selective enrichment in the tumor epithelium positions CD155 as a promising therapeutic target for both checkpoint inhibition and epithelial-directed approaches in cervical cancer.

INTRODUCTION

Cervical cancer remains a major global health concern, with recent estimates reporting approximately 662,000 new cases and 349,000 deaths annually, ranking it among the most prevalent and lethal malignancies affecting women worldwide.[1] While human papillomavirus (HPV) vaccination and screening programs have significantly improved prevention, a substantial global disease burden remains. The near-universal association of cervical cancer with oncogenic HPV infection, marked by the expression of immunogenic viral antigens such as E6 and E7, combined with a relatively high mutational burden and dense immune infiltration, suggests an immunogenic tumor profile and provides a strong rationale for immunotherapeutic approaches.[2–4] However, despite this promising biology, clinical responses to current immunotherapies remain limited. Programmed cell death protein 1 (PD-1) blockade with pembrolizumab is approved for programmed death-ligand 1 (PD-L1)-positive advanced cervical cancer, defined by a combined positive score ≥1, yet objective overall response rates remain below 20%, while durable benefit is limited to a subset of patients.[5 6] These limitations highlight the need to better understand the immune landscape of cervical cancer to uncover alternative, targetable immunoregulatory pathways.

To address this gap, we performed an integrative spatial and transcriptomic analysis of the cervical cancer immune microenvironment. Using immunohistochemistry (IHC) across distinct tumor niches and transcriptomic data from The Cancer Genome Atlas (TCGA), we profiled immune subset and checkpoint markers, many of which remain understudied in cervical cancer. Our dual-cohort approach aimed to define the immunoregulatory architecture of cervical cancer and identify actionable immune escape mechanisms beyond the PD-L1/PD-1 axis.

MATERIALS AND METHODS

Patient selection, tissue sampling, and data retrieval

Formalin-fixed, paraffin-embedded (FFPE) tumor tissue samples from 65 patients with cervical cancer diagnosed between October 2009 and November 2021 were retrospectively collected from the tumor biobanks of Antwerp University Hospital (Edegem, Belgium) and ZAS Sint-Augustinus Hospital (Antwerp, Belgium). Sample selection was based on a review of electronic medical records to confirm a diagnosis of cervical cancer and the availability of clinicopathological data. Only cases with squamous cell carcinoma or HPV-associated adenocarcinoma were included; tumors with adenosquamous carcinoma or other histotypes, including HPV-independent adenocarcinoma variants, were excluded. All tissue samples were obtained via hysterectomy, trachelectomy, conization, or biopsy, fixed in 4% neutral-buffered formaldehyde for up to 48 hours, and routinely processed for paraffin embedding. An additional inclusion criterion was the presence of sufficient tumor tissue in FFPE samples to permit multiple sectioning for immunohistochemical analysis.

Clinicopathological variables retrieved from medical records included date of diagnosis, histotype, Fédération Internationale de Gynécologie et d'Obstétrique (FIGO) stage, differentiation grade, HPV status, lymphovascular invasion, smoking history, date of relapse, and date of death. Disease stage was categorized consistent with the FIGO classification system: early-stage disease was defined as IA1 to IB1 (FIGO 2009) or IA1 to IB2 (FIGO 2018); locally advanced cervical cancer as IB2 to IVA (2009) or IB3 to IVA (2018); and recurrent or metastatic disease as stage IVB. Progression-free survival (PFS) was defined as the time from diagnosis to the date of documented relapse. Patients without relapse were censored at the date of last follow-up. Overall survival (OS) was defined as the time from diagnosis to death from any cause. Patients who were still alive at last follow-up were censored at that date.

Immunohistochemistry

IHC was performed on 5 µm thick FFPE tissue sections. Slides were baked at 60°C for 1 hour to promote tissue adherence and soften paraffin. All staining procedures were performed on Dako Autostainer Link 48 or Dako Omnis platforms (Agilent Technologies, Santa Clara, California, USA), using the EnVision FLEX system in combination with the PT Link module for antigen retrieval. Heat-induced epitope retrieval was performed at 97°C using either high-pH (pH 9; Agilent #GV804) or low-pH (pH 6; Agilent #GV805) retrieval buffer, depending on the target antigen. Visualization was achieved using either 3,3′-diaminobenzidine (Agilent #GV825) or HRP Magenta (Agilent #GV925) chromogens, followed by automated hematoxylin counterstaining. Coverslipping was performed manually or using the Dako CoverStainer (Agilent). Human tonsil and appendix tissues served as positive controls and were included in each staining run to verify antibody specificity and staining consistency. Details on all antibodies and short protocols are provided in online supplemental table 1.

Immunohistochemical scoring and interpretation

All stained slides were independently evaluated in a blinded manner by two experienced pathologists and one trained scientist. As adjacent normal epithelial tissue was often absent or insufficiently represented for meaningful comparison, our analysis focused exclusively on the tumor

area, with peritumoral normal tissue explicitly excluded from interpretation. Within the tumor region, two intratumoral niches were delineated and scored separately: the tumor stroma (TS) and the tumor epithelium (TE). Scoring was performed for both immune subset markers (CD4-CD8 double stain, CD4-FoxP3 double stain, CD68, and NKp46) and immune checkpoint markers (HLA-E, CD47, CD73, CD276, CD155, Gal-9, PD-L1, CD70, and LAG-3). Immune marker expression was quantified as the percentage of positive cells within each tumor niche. For immune subset markers, TS scores were visually estimated as the proportion of positive stromal cells among total nucleated TS cells. For TE scoring, the percentage of positive immune cells was estimated relative to total tumor cells, recognizing that tumor cells are not expected to express these markers. For immune checkpoint markers, positivity was similarly quantified as the percentage of positive cells among all cells in the respective tumor niche. A sample was considered positive if at least 1% of cells in the evaluated tumor niche demonstrated specific staining, regardless of intensity or distribution.[7] Tumor immunotypes were further categorized for each patient based on CD8 staining patterns: desert ($CD8^+$ cells <5% in both TS and TE), excluded (≥5% in TS and <5% in TE), and inflamed (≥5% in both niches).[8] Any scoring discrepancies were resolved by joint review and consensus. Whole-slide images of selected sections were acquired using an IntelliSite Ultra-Fast Scanner (Philips, Amsterdam, the Netherlands) at 40x magnification to generate high-resolution representative images.

Data sources and cohorts

Cervical cancer transcriptomic and clinical data were retrieved in March 2025 from multiple repositories, including TCGA, the Genotype-Tissue Expression (GTEx) Project, and the Belgian Cancer Registry (BCR). TCGA messenger RNA expression and corresponding clinical data for the cervical squamous cell carcinoma and endocervical adenocarcinoma collection (CESC) were obtained via the cBioPortal platform (https://www.cbioportal.org).[9 10] The dataset included both transcripts per million-normalized expression values, sourced from the Genomic Data Commons, and RNA-Sequencing by Expectation Maximization (RSEM) data from the Firehose Legacy pipeline. The final TCGA cohort comprised 304–306 patients, depending on data completeness for each specific analysis. Immune cell composition was assessed using CIBERSORT-estimated immune cell fraction data for the TCGA cervical cancer cohort (TCGA-CESC; n=304), obtained from the Tumor Immune MicroEnvironment DataBase (https://timedb.deepomics.org).[11] Normal cervical tissue gene expression data were retrieved from the GTEx Project, Analysis Release V.10 (https://www.gtexportal.org; dbGaP accession phs000424.v10.p1).[12] Bulk RNA-sequencing data from 23 ectocervical and 24 endocervical tissue samples were merged to generate a combined dataset of 47 histologically normal cervical tissue specimens, used as a non-malignant reference group. Population-level clinical data were obtained from the 2022 Cervical Cancer Fact Sheet published by the BCR (https://kankerregister.org), providing national epidemiological context for the Belgian patient population represented in our IHC cohort. To assess treatment response, three chemotherapy resistance signatures (Fang,[13] Olaussen,[14] Aldonza[15]) and three immunotherapy response signatures (Ayers,[16] Hugo[17]) were retrieved from the literature, with signature scores calculated as the mean RSEM expression of all genes per signature.

Cell lines and culture conditions

HeLa cervical cancer cells were obtained from the American Type Culture Collection (Manassas, Virginia, USA) and cultured in Dulbecco's Modified Eagle Medium (Thermo Fisher #10938025) supplemented with 10% fetal bovine serum (FBS, Thermo Fisher #10270106) and 2 mM L-glutamine. NK-92 cells were obtained from the German Collection of Microorganisms and Cell Cultures (DSMZ, Braunschweig, Germany) and cultured in GlutaMAX alpha minimum essential medium (Life Technologies #32561037) supplemented with 12.5% FBS, 12.5% horse serum (Thermo Fisher #16050122), 2 mM L-glutamine, 1% penicillin/streptomycin (Thermo Fischer #15140), and 150 U/mL recombinant human interleukin-2 (IL-2; ImmunoTools #11340027), as previously described.[18] Cell cultures were maintained in exponential growth phase at 37°C in a humidified incubator with 5% CO_2, confirmed to be *Mycoplasma*-free using the MycoAlert Detection kit (Lonza #LT07-318), and validated by short tandem repeat profiling.

Co-culture killing assay

HeLa cells were transduced with mKate2 nuclear reporter using the Incucyte NucLight Red lentivirus (EF1α promoter, bleomycin-selectable; Sartorius #4478) at a multiplicity of infection of three using TransDux MAX reagent (System Biosciences #LV860A-1), followed by sorting of $mKate2^+$ populations using a BD FACSAria II cell sorter (BD Biosciences, Franklin Lakes, New Jersey, USA). Cells were harvested and seeded at 2.5×10^3 cells per well in 384-well plates in 30 µL NK-92 medium without IL-2. At least 6 hours after seeding, once tumor cells were adherent, treatments were added using a D300e Digital Dispenser (Tecan Life Sciences, Männedorf, Switzerland). Treatments included tiragolumab (Selleckchem #A2028), anti-CD155 (aCD155; Bio-Rad #MCA4644EL), enoblituzumab (Selleckchem #A2626), magrolimab (Selleckchem #A2036), cusatuzumab (Selleckchem #A2747), oleclumab (Selleckchem #A2611), cobolimab (Selleckchem #A2802), monalizumab (Selleckchem # A2053), and pembrolizumab (Selleckchem #A2005), as well as their isotype controls Hu IgG1 (Selleckchem #A2051), Mu IgG1 (BioLegend #400166), and Hu IgG4 (Selleckchem

#A2052). Treatments were applied at 10 µg/mL as calculated for a final co-culture volume of 50 µL. After overnight incubation at 37°C, 20 µL of NK-92 cells without IL-2 were added to establish co-cultures at an optimized effector-to-target ratio of 3:1. Tumor killing was monitored by live-cell imaging on a Spark Cyto multimode plate reader (Tecan Life Sciences) using the DrugVision.AI drug screening platform (University of Antwerp, Belgium), with images acquired at baseline (0 hours) and every 6 hours for 48 hours. Image and data analyses were performed with the Orbits Oncology platform (Orbits Oncology, San Francisco, USA).[19] Tumor cell killing was quantified from red object counts per well, normalized first to baseline, then to the corresponding tumor cell monoculture, and finally to the matched isotype control, yielding relative killing values.

Statistical analysis and data visualization

Pearson correlation coefficients were used to assess relationships between continuous variables, including clinical and molecular values across cohorts and to evaluate pairwise correlations between individual markers for patterns of co-expression or inverse association. The prognostic significance of clinicopathological parameters and marker expression data were evaluated using univariate Cox proportional hazards regression and log-rank tests, with survival curves generated by the Kaplan-Meier method. For categorical variables, Kaplan-Meier curves were stratified by group membership. For continuous variables, optimal cutoffs for dichotomization were identified using X-tile software V.3.6.1 (Yale University School of Medicine, New Haven, Connecticut, USA).[20] Comparative analyses of marker expression between tumor niches were conducted using the Wilcoxon signed-rank test. For clinicopathological subgroup comparisons, either the Mann-Whitney U test (for binary variables) or the Kruskal-Wallis test with pairwise comparison using Dunn's post hoc test with Bonferroni adjustment (for variables with more than two levels) was employed. For co-culture analyses, linear mixed-effects models were used as detailed in the corresponding figure footnote. To account for multiple hypothesis testing and control the false discovery rate, Benjamini-Hochberg correction was systematically applied. In analyses involving more than two groups, Benjamini-Hochberg-adjusted p values were calculated prior to post hoc testing, and only variables with statistically significant adjusted p values were subjected to further pairwise comparisons. A two-sided p value of <0.05 was considered statistically significant. All statistical analyses were conducted using R V.4.3.2 (R Foundation for Statistical Computing, Vienna, Austria), Python V.3.12.0 (Python Software Foundation, Wilmington, Delaware, USA), or JMP Pro V.17.2.0 (SAS Institute, Cary, North Carolina, USA). Data visualization was performed using GraphPad Prism V.10.4.2 (GraphPad Software, Boston, Massachusetts, USA) and Python-based libraries, including Pandas, NumPy, SciPy, Seaborn, Matplotlib, Statsmodels, Scikit-learn, and scikit-posthocs.

RESULTS

Cross-platform and real-world cohort alignment underscore the translational relevance of the study

To evaluate the comparability and real-world representativeness of our IHC (n=65) and TCGA (n=306) cohorts, we systematically assessed patient demographics and clinicopathological characteristics (table 1). All patients were treatment naïve for cervical cancer at sample collection. Median age at diagnosis was 49.8 years (IHC) and 46.0 years (TCGA), with age distributions moderately to strongly correlated (Pearson r=0.7193) and reflective of the national profile from the BCR (figure 1A–B and online supplemental figure 1A). Squamous cell carcinoma (SCC) was the predominant histotype, observed in 72.3% (IHC) and 82.7% (TCGA), while adenocarcinoma (AC) accounted for 27.7% and 17.3%, respectively. Approximately half of the patients in each cohort had FIGO stage I disease, with early stages (FIGO I-II) more frequent in the TCGA (77.3%) than IHC (67.7%) cohort (table 1 and figure 1C). FIGO distributions were consistent with population-level data, with the IHC cohort showing slightly closer alignment (online supplemental figure 1A). Most tumors were moderately differentiated. All tumors in the IHC cohort were classified as HPV-associated, except for one SCC case with a negative PCR result. HPV subtype data were largely unavailable in this cohort, but among known cases, types 16 and/or 18 predominated. In contrast, HPV subtype annotation in TCGA was available for most cases and similarly demonstrated a predominance of HPV 16 and/or 18 types, with a small subset annotated as HPV-negative. Lymphovascular invasion data were incomplete but comparable between cohorts (58.2% IHC; 53.3% TCGA). Survival analyses showed similar patterns across cohorts. Among patients with follow-up data, relapse occurred in 27.9% (IHC) and 18.1% (TCGA), with a mean PFS of 5.6 and 2.8 years, and 5-year PFS rates of 71.9% and 64.5%, respectively. At the time of analysis, death had occurred in 31.7% (IHC) and 23.9% (TCGA), with a mean OS of 6.5 and 2.9 years, and 5-year OS rates of 73.8% and 69.0%, respectively. Prognostic impacts of clinicopathological parameters were consistent with clinical expectations (figure 1D–E and online supplemental figures 1B,2). Finally, to evaluate cross-platform concordance, we compared protein-level expression (IHC) with transcript-level expression (TCGA) for key immune markers (figure 1F). Expression levels were strongly correlated (Pearson r=0.8560), demonstrating robust agreement between datasets (figure 1G).

Together, these findings show that both study cohorts are demographically and clinically representative of the broader cervical cancer population and their molecular profiles are highly concordant across platforms, providing

Table 1 Demographics and clinicopathological characteristics of the study cohorts

Patient characteristics	IHC cohort (n=65)		TCGA cohort (n=306)	
Age at diagnosis (years)				
Mean±SD	50±11.9		48±13.8	
Range	22–75		20–88	
Histological diagnosis				
Squamous cell carcinoma	47	(72.3%)	253	(82.7%)
Adenocarcinoma	18	(27.7%)	47	(15.4%)
Adenosquamous carcinoma	0	(0.0%)	6	(2.0%)
FIGO stage*				
I	34	(52.3%)	162	(52.9%)
II	10	(15.4%)	69	(22.6%)
III	8	(12.3%)	46	(15.0%)
IV	13	(20.0%)	22	(7.2%)
Unknown	0	(0.0%)	7	(2.3%)
Disease stage				
Early stage	32	(49.2%)	123	(40.2%)
Locally advanced	25	(38.5%)	163	(53.3%)
Recurrent/ metastatic	8	(12.3%)	13	(4.2%)
Unknown	0	(0.0%)	7	(2.3%)
Differentiation grade				
G1: Well-differentiated	9	(13.8%)	19	(6.2%)
G2: Moderately differentiated	28	(43.1%)	135	(44.1%)
G3: Poorly differentiated	23	(35.4%)	119	(38.9%)
G4: Undifferentiated	0	(0.0%)	1	(0.3%)
Unknown	5	(7.7%)	32	(10.5%)
HPV association				
HPV-associated	64	(98.5%)	282	(92.2%)
HPV-independent	1	(1.5%)	22	(7.2%)
Unknown	0	(0.0%)	2	(1.0%)
HPV subtype				
HPV 16 and/or 18	19	(29.2%)	210	(68.6%)
Other HPV type(s)	6	(9.2%)	71	(23.2%)
Negative	1	(1.5%)	22	(7.2%)
Unknown	39	(60.0%)	3	(1.0%)
Lymphovascular invasion				
Yes	32	(49.2%)	81	(26.5%)
No	23	(35.4%)	71	(23.2%)
Unknown	10	(15.4%)	154	(50.3%)
Smoker				
Yes	25	(38.5%)	119	(38.9%)
No	31	(47.7%)	144	(47.1%)
Unknown	9	(13.8%)	43	(14.0%)
Relapse				
Yes	17	(26.2%)	48	(15.7%)
No	43	(66.1%)	217	(70.9%)
Unknown	5	(7.7%)	41	(13.4%)
Dead				
Yes	20	(30.8%)	73	(23.9%)
No	43	(66.1%)	233	(76.1%)
Unknown	2	(3.1%)	0	(0.0%)
PFS (years)				
Mean±SD	5.6±4.0		2.8±3.2	
Range	0.2–14.5		0.005–17.5	
5-year PFS	71.94%		64.49%	
OS (years)				
Mean±SD	6.5±3.7		2.9±3.1	
Range	0.2–14.5		0.005–17.5	
5-year OS	73.77%		69.03%	

*FIGO stage according to the classification system in use at the time of diagnosis.
FIGO, Fédération Internationale de Gynécologie et d'Obstétrique; HPV, human papillomavirus; IHC, immunohistochemistry; OS, overall survival; PFS, progression-free survival; TCGA, The Cancer Genome Atlas.

a solid foundation for downstream comparative and integrative analyses.

Immune subsets localize to the tumor stroma in cervical cancer

To characterize the spatial distribution and inter-patient variability of immune subsets in cervical cancer, we performed detailed IHC analysis of tumor tissues, complemented by TCGA transcriptomic profiling (figure 2). We selected CD4, CD8 (*CD8A*), CD68, FoxP3, and NKp46 (*NCR1*) as representative markers of key immune subsets. Analyses focused on the tumor area, excluding peritumoral stroma, with separate assessment of two intratumoral niches: the TS and TE (online supplemental figure 3A). IHC illustrated distinct staining patterns (figure 2A). Across all markers, immune subset densities were significantly higher in the TS than in the TE (figure 2B and online supplemental table 2). In the TS, $CD8^+$ (28%) and total $CD4^+$ (27%) cells were most abundant, followed by $CD68^+$ (16%), $CD4^+FoxP3^+$ (13%), and $NKp46^+$ (5%) cells. In the TE, $CD8^+$ (10%) and $CD68^+$ (8%) cells predominated. Principal component analysis of mean-imputed and standardized immune marker expression profiles from the TE and TS of individual patients confirmed clear segregation

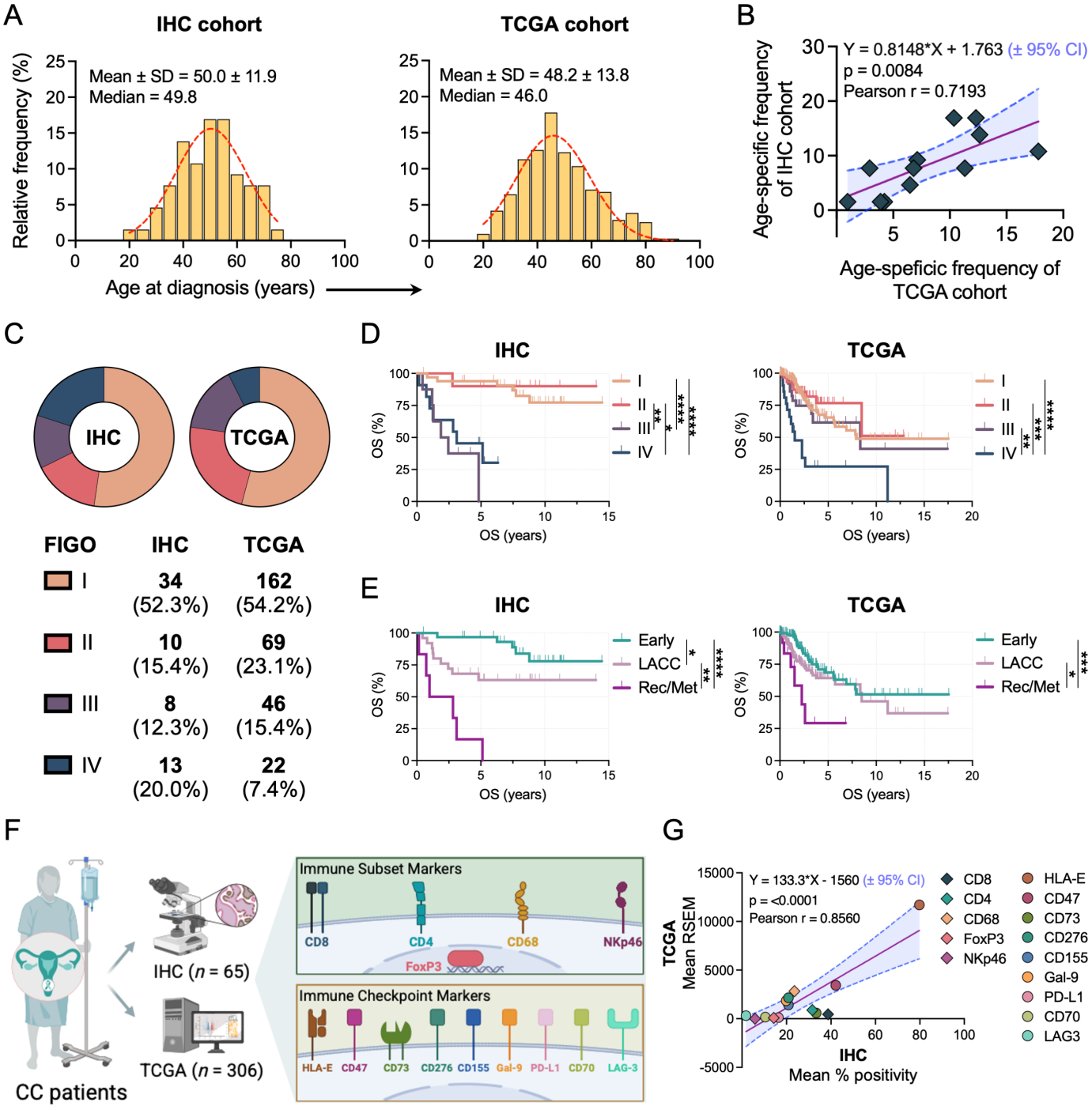

Figure 1 Study cohorts reflect real-world cervical cancer profiles with cross-platform consistency. (A) Age distribution at diagnosis for the IHC cohort (left) and TCGA cohort (right). (B) Correlation of age distributions between the two study cohorts, showing a moderate to strong positive Pearson correlation. Each data point represents an age group as depicted in panel A. (C) FIGO stage distributions presented as pie charts (top) and corresponding absolute counts and relative proportions (bottom) for both cohorts. (D–E) Kaplan-Meier survival curves of OS, stratified by (D) FIGO stage and (E) disease stage, illustrating consistent prognostic trends across cohorts. (F) Schematic overview of the study design, illustrating the integration of multi-omics analyses across IHC and TCGA cohorts. Figure created using BioRender (https://www.biorender.com). (G) Correlation of immune marker expression levels between protein (IHC) and transcriptomic (TCGA) data, demonstrating strong concordance. Statistical significance was determined using two-tailed Pearson correlation tests for correlation analyses and log-rank tests for survival comparisons, both with Benjamini-Hochberg correction applied for multiple testing. Significance levels are indicated as follows: *p<0.05, **p<0.01, ***p<0.001, and ****p<0.0001. CC, cervical cancer; FIGO, Fédération Internationale de Gynécologie et d'Obstétrique; IHC, immunohistochemistry; LACC, locally advanced cervical cancer; OS, overall survival; Rec/Met, recurrent or metastatic disease; RSEM, RNA-Sequencing by Expectation Maximization; TCGA, The Cancer Genome Atlas.

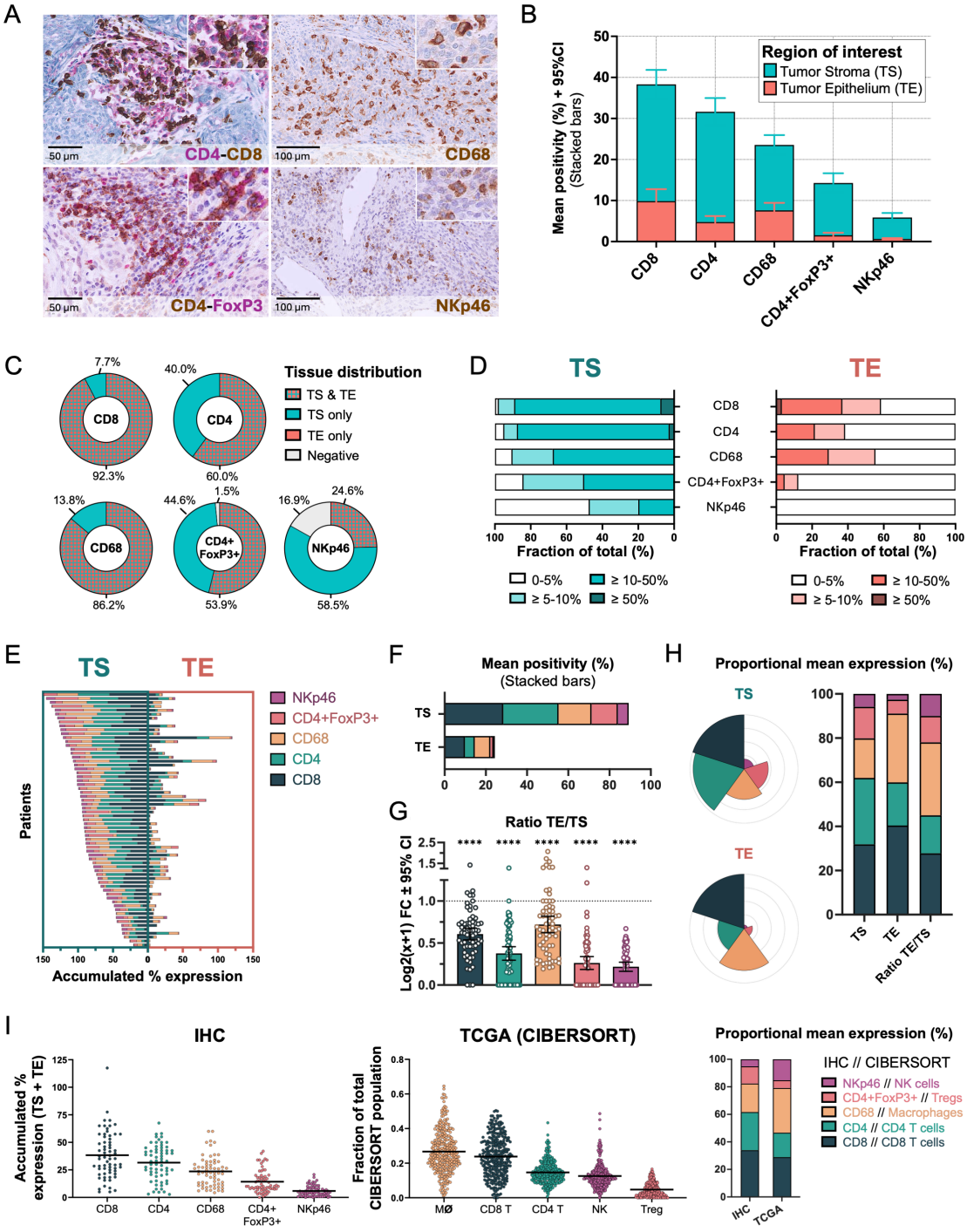

Figure 2 Transcriptomic immune subset abundance localizes primarily to the tumor stroma in spatial proteomic analysis. (A) Representative IHC images of immune subset markers in cervical cancer tissues. (B) Stacked bar plots of mean expression levels for each immune subset in TS and TE, based on IHC scoring. (C) Pie charts depicting spatial distribution of marker expression across TS and TE niches, with positivity scored as ≥1%. (D) Distribution of expression levels per marker in TS and TE, stratified by defined thresholds. (E) Stacked immune subset expression per patient across TS and TE niches, ordered by accumulated TS expression (sum of %-positivity of each marker). (F) Mean expression fractions per immune subset in each tumor niche. (G) Mean ratio of TE-to-TS expression levels for individual markers. Asterisks indicate statistically significant enrichment in the TS niche (ratio <1) for all immune subset markers. (H) Proportional mean expression of immune subsets visualized as concentric circular wedge plots (left) and bar graphs (right), highlighting relative shifts between tumor niches. (I) Comparison of accumulated protein-level IHC expression (sum of %-positivity in TS and %-positivity in TE) with CIBERSORT-inferred immune cell proportions from TCGA transcriptomic data, visualized as mean expression levels (left) and relative proportions (right). Statistical significance for tumor niche comparisons was assessed using two-tailed Wilcoxon-signed rank tests with Benjamini-Hochberg correction applied for multiple testing. Significance levels are indicated as follows: *p<0.05, **p<0.01, ***p<0.001, and **** p<0.0001. FC, fold change; IHC, immunohistochemistry; MØ, macrophages; NK, natural killer cells; TCGA, The Cancer Genome Atlas; TE, tumor epithelium; Treg, regulatory T cells; TS, tumor stroma.

between the two niches, underscoring distinct immune microenvironments (online supplemental figure 3B). These were further supported by volcano plot analysis, demonstrating significant TS enrichment for all immune subset markers (online supplemental figure 3C). Nearly all tumors exhibited detectable immune infiltration in at least one niche, except for NKp46$^+$ cells, which were undetectable or expressed at very low levels (<1%) in 16.9% of cases (figure 2C). In the TS, all subset markers except NKp46 reached high levels (≥10% positivity) in more than 50% of cases (figure 2D). In contrast, immune infiltration in the TE was generally sparse, with CD8$^+$ and CD68$^+$ cells most frequently detected (in 92.3% and 86.1% of cases, respectively), while NKp46$^+$ cells were rare, detected in only 24.6% of cases and never exceeding 5% positivity (figure 2C–D).

Despite overall trends, immune infiltration patterns varied between patients (figure 2E). While mean expression consistently favored the TS, a minority of tumors exhibited greater immune subset presence in the TE (figure 2E–G). Comparative analysis of tumor niche-specific proportions revealed a relative redistribution of CD8$^+$ and CD68$^+$ cells toward the epithelial niche, which may suggest their involvement in direct tumor engagement (figure 2H). To validate the IHC findings, we compared accumulated protein expression with transcriptomic data from TCGA. Immune cell deconvolution using CIBERSORT revealed similar trends, though it showed macrophages as the most abundant subset, whereas CD68$^+$ cells ranked third in IHC (figure 2I). NKp46 (*NCR1*) was the lowest-expressed subset marker in both cohorts (online supplemental figure 3D). Interestingly, CIBERSORT deconvolution demonstrated more natural killer (NK) cells than regulatory T cells, likely reflecting differences in marker sensitivity and broader gene signature used for NK cell estimation.

Collectively, these findings highlight the preferential enrichment of immune subsets in the TS over TE and reveal marked inter-patient heterogeneity in immune infiltration patterns, emphasizing the spatial and inter-individual complexity of the cervical cancer immune landscape.

Alternative immune checkpoints surpass PD-L1 expression with tumor niche-specific patterns

Building on our spatial and inter-patient characterization of immune subset markers, we next examined immune checkpoint expression patterns to further define the immunoregulatory landscape of cervical cancer (figure 3). Given the limited clinical efficacy of anti-PD-1, the sole approved immunotherapy for cervical cancer, we prioritized alternative checkpoints—HLA-E, CD47, CD73 (*NT5E*), CD276, CD155 (*PVR*), Galectin-9 (Gal-9, *LGALS9*), CD70, and LAG-3—based on their established roles in immune modulation, limited exploration in cervical cancer, and availability of clinically actionable compounds targeting their pathways.

IHC revealed distinct staining patterns and niche-specific localization of immune checkpoint markers (figure 3A–B and online supplemental table 2). HLA-E exhibited the highest expression overall (TS: 39%, TE: 41%), followed by CD47 (TS and TE: 21%). In contrast, PD-L1 expression was low (TS: 5%, TE: 11%). Most immune checkpoint markers were detected in over 75% of patients, whereas LAG-3, the only receptor in our panel, was absent or minimally expressed (<1%) in 76.9% of cases, likely reflecting its transient, activation-dependent expression compared with more stably expressed ligands (figure 3C). Among cases with >5% checkpoint expression, more than 50% showed high levels (≥10%) for nearly all markers (figure 3D). Like immune subset markers, checkpoints exhibited considerable inter-patient variability (figure 3E). Overall, expression levels were slightly higher in the TE niche, with several markers showing a strong preference for specific tumor niches: CD276 and CD155 were selectively enriched in the TE, whereas CD73 and CD70 were more prominent in the TS (figure 3F–H and online supplemental figure 3C). To assess the robustness of the IHC-derived findings, accumulated protein-level expression was compared with transcriptomic data from TCGA. Similar trends were observed across platforms, with *HLA-E* and *CD47* emerging as the most abundantly expressed immune checkpoints, and *CD274*, the gene encoding PD-L1, the lowest (figure 3I). Notably, despite high expression across platforms, *HLA-E* expression did not differ between tumor and normal cervical tissue (online supplemental figure 3E). Similarly, *CD276* was selectively enriched in the TE, but not elevated relative to normal tissue. In contrast, *PVR* (CD155), the other TE-enriched marker, showed significantly higher expression in tumors. *CD47*, *LGALS9*, *CD70*, and *CD274* were also significantly upregulated in tumor samples, while *NT5E* was higher expressed in normal cervical tissue.

Overall, these findings reveal a heterogeneous yet frequently abundant immune checkpoint landscape in cervical cancer, with PD-L1 consistently surpassed by alternative checkpoints organized in distinct tumor niche-specific patterns.

Cross-platform correlation analysis reveals consistent immune subset relationships with selective LAG-3 associations

To explore immunological relationships, we investigated co-expression patterns among immune subset and checkpoint markers by performing pairwise correlation analyses on both IHC-derived protein expression data and TCGA-based transcriptomic data (online supplemental figure 4). Correlation matrices revealed limited overall concordance between protein-level and gene-level datasets, with only a few marker pairs exhibiting strong and statistically significant correlations across both platforms (online supplemental figure 4A). Notably, the highest cross-platform consistency was observed among immune subset markers, suggesting biologically robust relationships that are preserved at both the protein and transcript

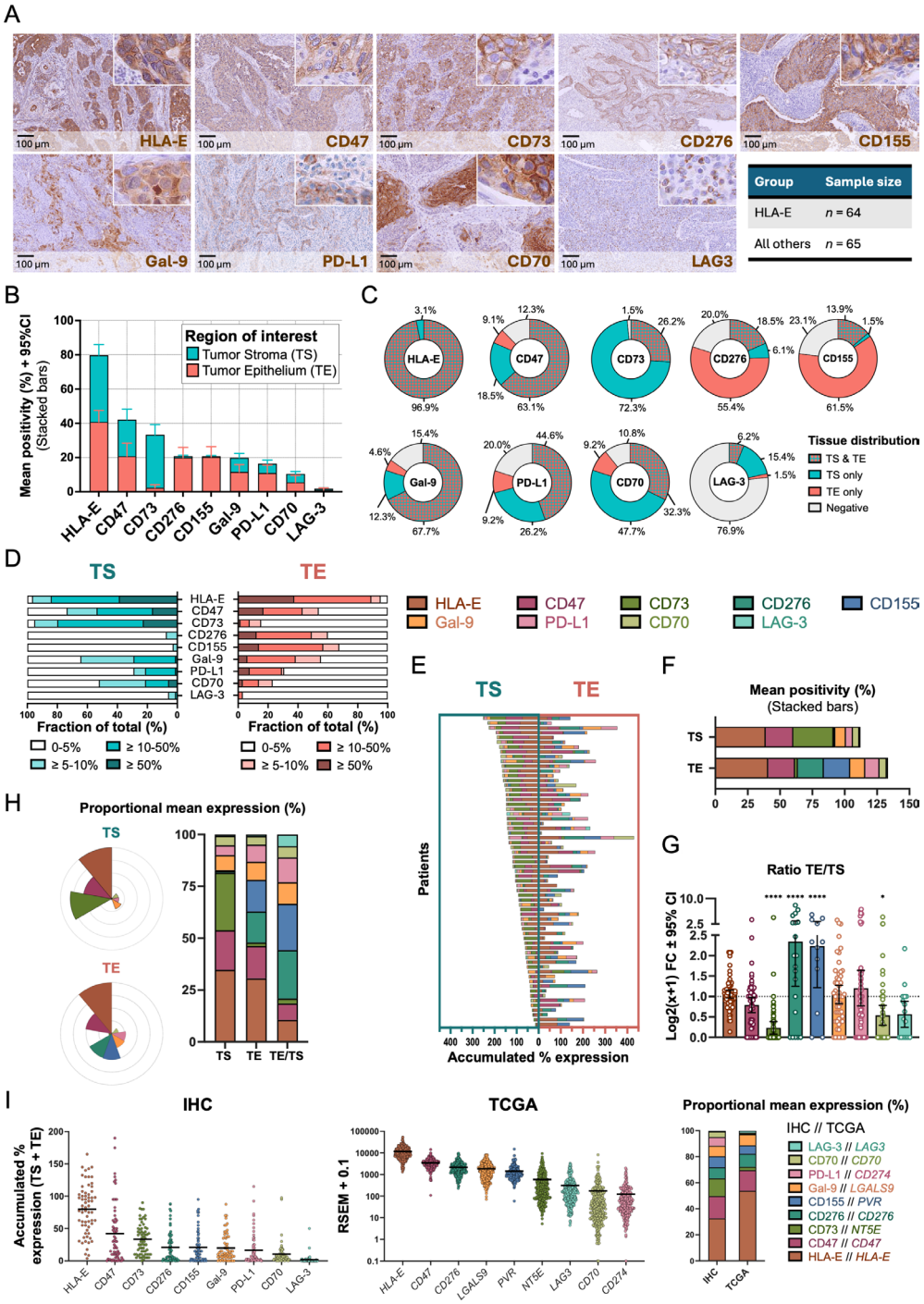

Figure 3 Immune checkpoint profiling reveals higher expression than PD-L1 in niche-specific spatial patterns. (A) Representative IHC images of immune checkpoint markers in cervical cancer tissues. (B) Stacked bar plots of mean expression levels for each immune checkpoint in the TS and TE, based on IHC scoring. (C) Pie charts illustrating the spatial distribution of marker expression across TS and TE niches, with positivity scored as ≥1%. (D) Distribution of expression levels for each marker in TS and TE, stratified by predefined thresholds. (E) Stacked immune checkpoint expression per patient across tumor niches, ordered by accumulated TS expression (sum of %-positivity of each marker). (F) Mean expression fractions of immune checkpoints in TS and TE. (G) Mean TE-to-TS expression ratios for individual markers. Asterisks indicate statistically significant enrichment in either the TS (ratio <1) or TE (ratio >1) niche. (H) Proportional mean expression visualized as concentric circular wedge plots (left) and corresponding bar graphs (right). (I) Comparison of accumulated protein-level IHC expression (sum of %-positivity in TS and %-positivity in TE) with transcriptomic data from TCGA, visualized as mean expression levels (left) and relative proportions (right). Statistical significance for tumor niche comparisons was assessed using two-tailed Wilcoxon signed-rank tests with Benjamini-Hochberg correction applied for multiple testing. Significance levels are indicated as follows: *p<0.05, **p<0.01, ***p<0.001, and ****p<0.0001. FC, fold change; IHC, immunohistochemistry; PD-L1, programmed death-ligand 1; RSEM, RNA-Sequencing by Expectation Maximization; TCGA, The Cancer Genome Atlas; TE, tumor epithelium; TS, tumor stroma.

levels (online supplemental figure 4B). In contrast, pairwise correlations between immune checkpoint markers were generally weak and not consistently replicated across datasets, limiting their interpretability. Interestingly, despite its low expression levels, LAG-3 consistently showed positive associations with CD8, CD4, and CD68 across both platforms, with its CD8 correlation emerging as particularly strong. This reproducible pattern may indicate coordinated upregulation of LAG-3 in cytotoxic T cell-rich tumor environments, potentially reflecting a role in adaptive immune regulation or T cell exhaustion.

Together, these findings suggest that while overall co-expression patterns vary between platforms, immune subset relationships are consistently preserved, and the reproducible association between LAG-3 and cytotoxic and myeloid markers highlights its potential relevance within immune-active tumor microenvironments.

Histotype-associated immune architectures reveal upregulated immune marker expression in squamous cell carcinoma

To contextualize immune marker expression to clinical features, we evaluated associations between both protein-level and gene-level data and key clinicopathological parameters (figure 4). Expression analysis across binary clinical variables revealed distinct immunological profiles linked to specific patient and tumor characteristics (figure 4A). Although most immune markers did not significantly differ across variables, FIGO stage was associated with differential expression of CD155 in TS and Gal-9 in TE in the IHC cohort (online supplemental figure 5A). Among all parameters assessed, histotype emerged as the strongest and most consistent association with immune marker expression, correlating with multiple markers across both the IHC and TCGA datasets. Shared histotype-associated expression patterns were observed for CD4, CD68, FoxP3, Gal-9, and PD-L1, suggesting that tumor histotype could play a role in shaping the immune microenvironment (figure 4B). To explore this further, we identified markers that showed statistically significant histotype associations in either cohort (figure 4C). Overall, SCC exhibited higher expression of both immune subset and checkpoint markers than AC. Notably, all differences were observed in immune markers expressed within the TE, highlighting this niche as a key site of histotype-specific immune variation. One notable inconsistency was observed for Gal-9, which showed higher expression in SCC in the IHC dataset but was more strongly associated with AC in the TCGA data.

These observations collectively highlight histotype as a key correlate of immune marker expression in cervical cancer, associated with elevated immune subset and checkpoint profiles in SCC compared with AC.

Prognostic tumor immunotypes exhibit distinct immune landscapes with shared CD155 expression

Tumor immunotypes—categorized as immune-desert, immune-excluded, and immune-inflamed—are emerging as critical determinants of tumor immunogenicity, linked to immune checkpoint inhibitor response and prognosis across multiple cancers.[21–24] Analyzing immune marker expression by immunotype can thus elucidate immune evasion mechanisms and guide stratified immunotherapy (figure 5). In our IHC cohort, immunotypes were defined based on $CD8^+$ spatial distribution (figure 5A).[8] Immune-inflamed tumors were most prevalent (47.7% of cases), followed by immune-excluded (40.0%) and immune-desert (12.3%). Patients with immune-desert tumors exhibited significantly worse outcomes than those bearing immune-inflamed tumors, highlighting the prognostic relevance of immunotype stratification (figure 5B). Immunotype-specific profiling revealed significant variation in expression of all immune subset markers, except NKp46, and checkpoint markers including HLA-E, CD47, CD73, PD-L1, CD70, and LAG-3, depending on tumor niche (figure 5C). Immune-inflamed tumors consistently exhibited the highest expression of immune markers in both niches, whereas immune-desert tumors showed the lowest levels across all markers, with one exception (figure 5D). Notably, CD155 in the TE niche was substantially present across all immunotypes and ranked as the second highest marker-niche combination within the immune-desert phenotype. Moreover, it was the only parameter with peak expression in the immune-desert group, although this difference did not reach statistical significance (figure 5C and online supplemental figure 5B,C).

These findings reflect the immunological distinctions underlying the immunotype stratification and highlight its biological relevance and potential to inform therapeutic strategies in cervical cancer.

CD155 consistently stratifies patient prognosis across platforms

To evaluate the prognostic value of investigated immune markers, we conducted survival and correlative analyses in both IHC and TCGA datasets (figure 6A–F). In the IHC cohort, high expression of all immune subset markers except CD68 was significantly associated with improved OS and PFS in a niche-specific manner, consistent with their roles in antitumor immunity (figure 6A). Although these associations did not reach statistical significance in univariate Cox regression models, their expression was consistently associated with improved OS in the TCGA cohort (online supplemental figure 6A-C). Among checkpoint markers, CD155 emerged as the only one significantly associated with OS in the IHC cohort, with associations observed in both the TS and TE (figure 6B). While not confirmed by Cox regression, they were validated in TCGA, where high *PVR*—encoding CD155—correlated with poorer survival (figure 6C and online supplemental figure 6B). Notably, CD155 expression was highest in immune-desert tumors, a phenotype previously linked to inferior prognosis, suggesting a potential immunosuppressive role for CD155 across microenvironments (figure 5C and online supplemental figure 5C).

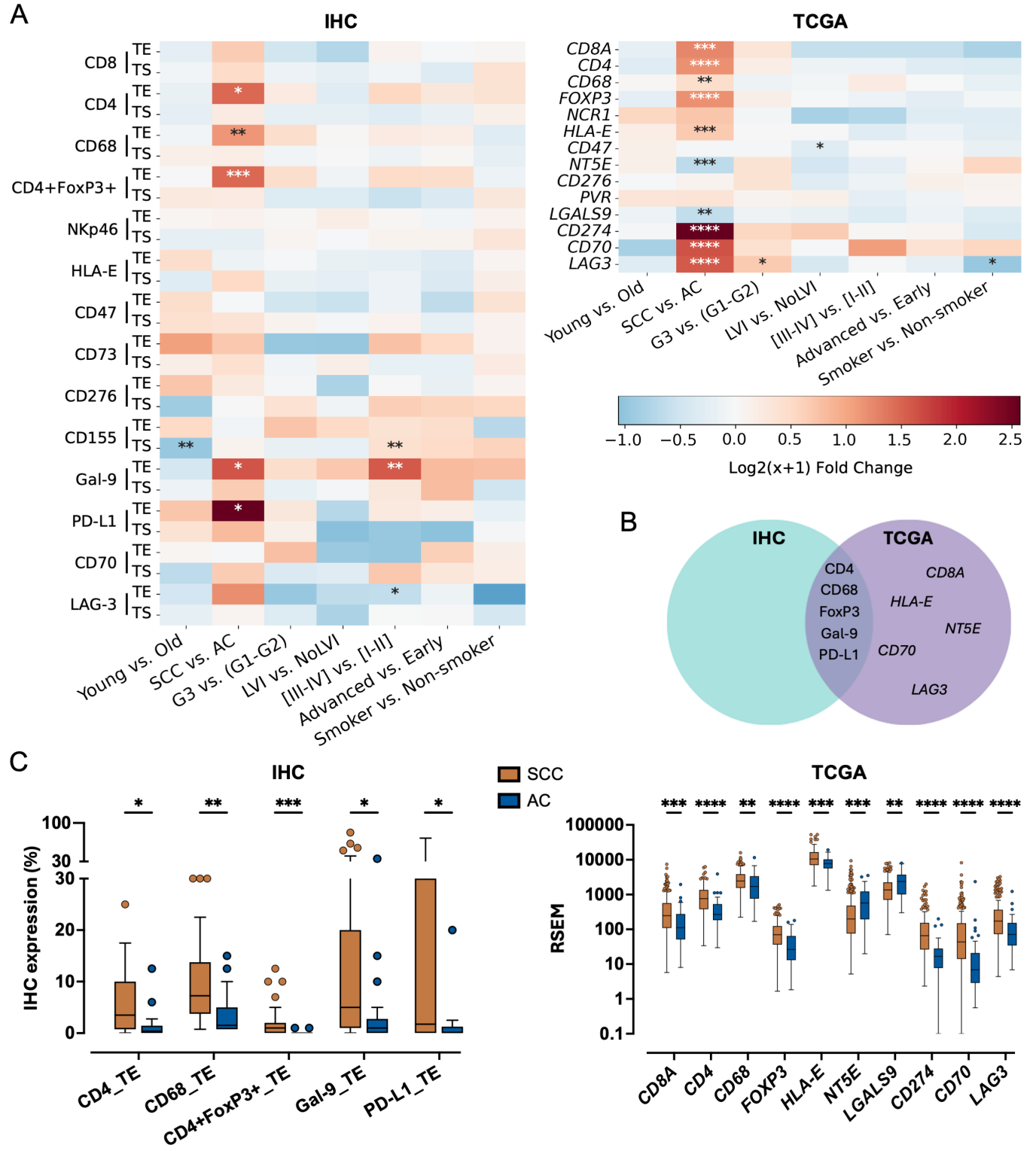

Figure 4 Cervical squamous cell carcinoma exhibits stronger immune marker expression than adenocarcinoma. (A) Heatmaps showing the $\log_2(x+1)$ fold changes in immune marker expression associated with binary clinicopathological variables in the IHC (left) and TCGA (right) cohorts. "Young"=age<median (49.8 years); "Old"=age≥median; "Early"=early-stage; "Advanced"=LACC and Rec/Met. (B) Venn diagram identifying overlapping and data-specific immune markers significantly associated with histotype. (C) Tukey boxplots illustrating subtype-specific expression patterns for selected immune markers in the IHC (left) and TCGA (right) cohorts. Statistical significance was assessed using two-tailed Mann-Whitney U tests with Benjamini-Hochberg correction applied for multiple testing. Significance levels are indicated as follows: *p<0.05, **p<0.01, ***p<0.001, and ****p<0.0001. AC, adenocarcinoma; FC, fold change; G1, well-differentiated; G2, moderately differentiated; G3, poorly differentiated; IHC, immunohistochemistry; LVI, lymphovascular invasion; PD-L1, programmed death-ligand 1; RSEM, RNA-Sequencing by Expectation Maximization; SCC, squamous cell carcinoma; TCGA, The Cancer Genome Atlas; TE, tumor epithelium; TS, tumor stroma.

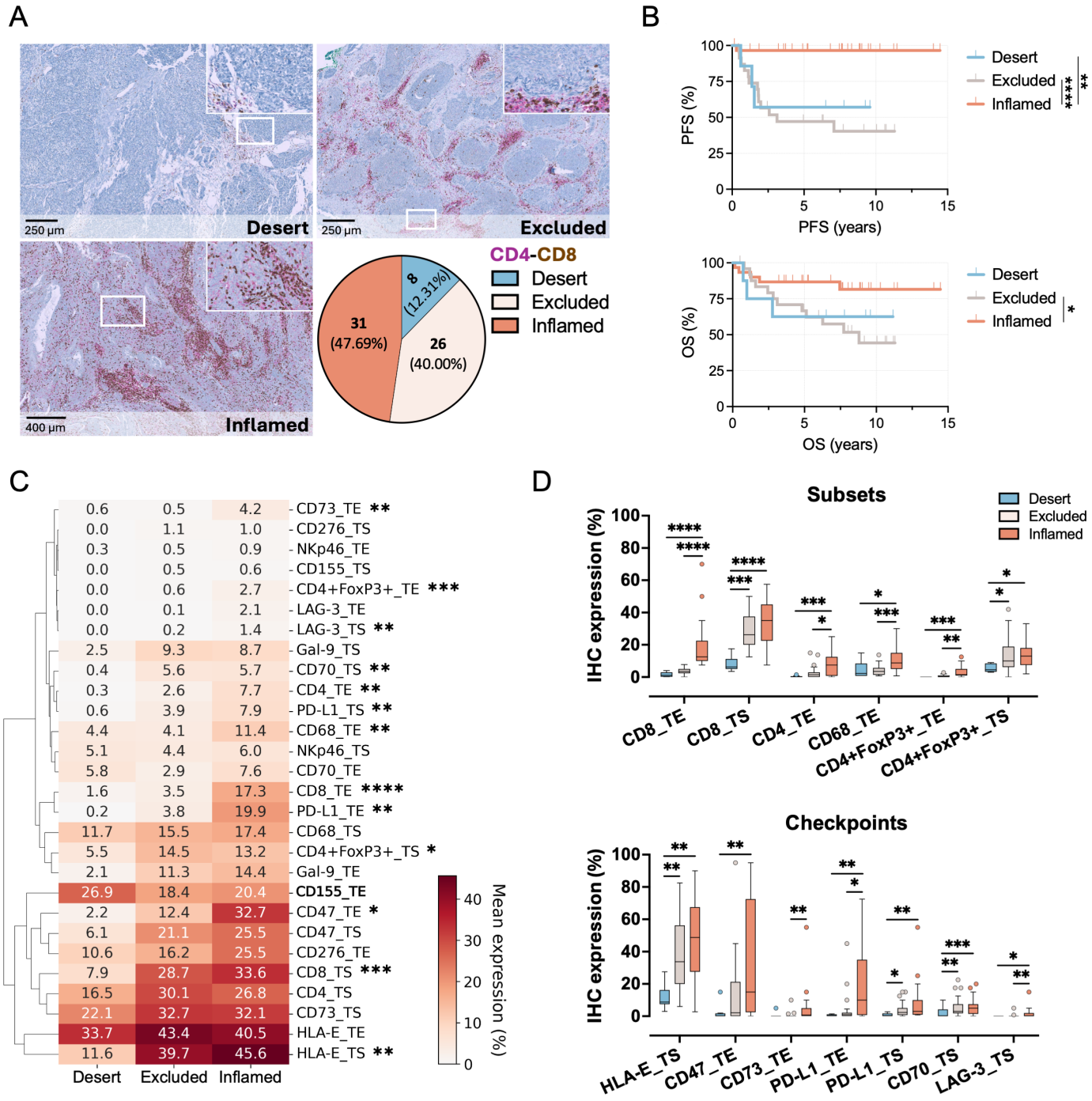

Figure 5 Tumor immunotypes show distinct prognostic and immune profiles while sharing CD155 expression. (A) Representative IHC images illustrating each tumor immunotype, along with their respective proportions within the IHC cohort. (B) Kaplan-Meier survival curves stratified by tumor immunotype, demonstrating the prognostic relevance of this classification in the IHC cohort. (C) Clustered heatmap showing the mean expression levels of all immune markers in the TS and TE, grouped by immunotype. (D) Tukey boxplots comparing marker expression across immunotypes for those markers showing statistically significant differences. Statistical significance was assessed using log-rank tests for survival comparisons and two-tailed Kruskal-Wallis tests for immunotype-based expression analysis, both with Benjamini-Hochberg correction applied for multiple testing. For markers with significant overall differences, pairwise immunotype comparisons were conducted using post hoc Dunn-Bonferroni testing. Significance levels are indicated as follows: * p<0.05, **p<0.01, ***p<0.001, and ****p<0.0001. HLA, human leukocyte antigen; IHC, immunohistochemistry; LAG-3, lymphocyte-activation gene 3; OS, overall survival; PD-L1, programmed death-ligand 1; PFS, progression-free survival; TE, tumor epithelium; TS, tumor stroma.

Supporting this, the T cell immunoreceptor with Ig and ITIM domains (TIGIT) axis indicated an immunosuppressive configuration in cervical tumors compared with normal tissue, with *TIGIT*, the primary inhibitory receptor for CD155, significantly upregulated in tumors, while the co-stimulatory receptor *CD226* (DNAM-1) showed

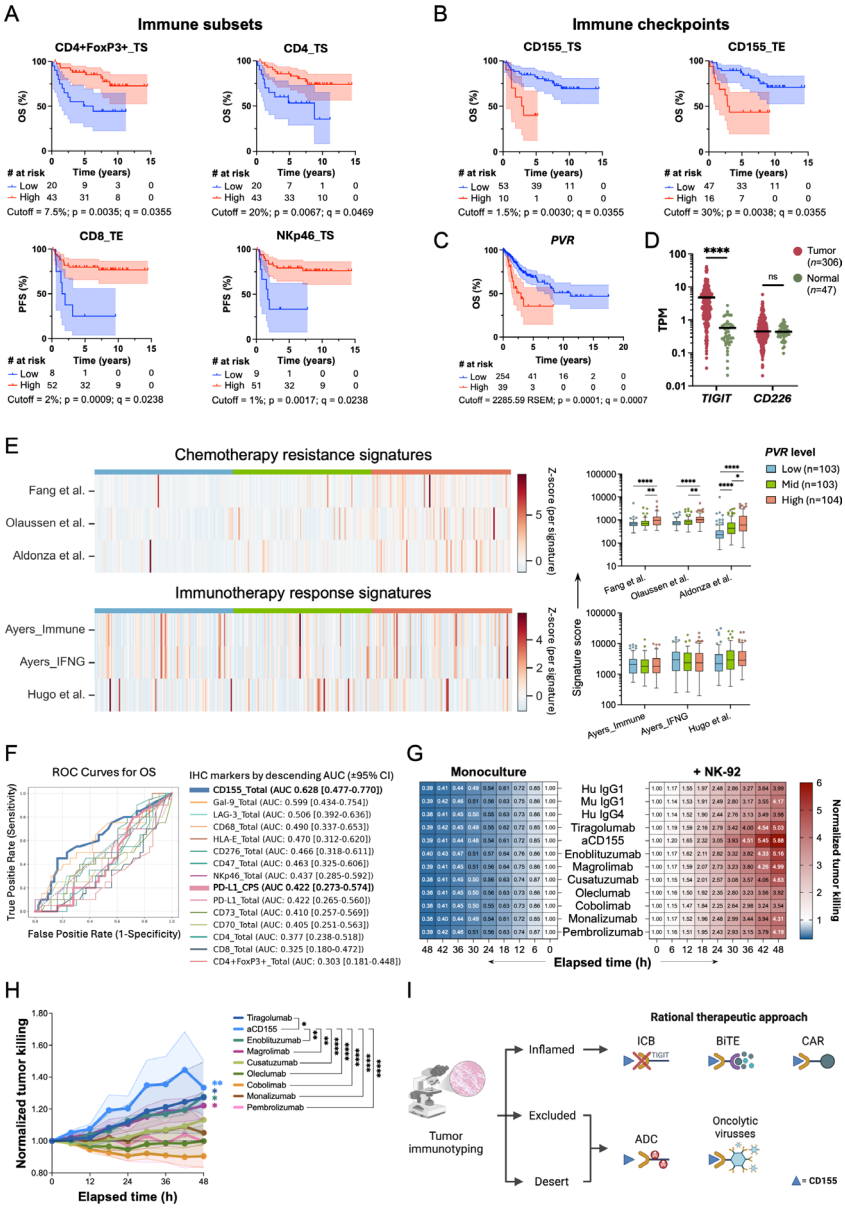

Figure 6 CD155 is a prognostic and functional therapeutic target in cervical cancer. (A) Kaplan-Meier curves of significant associations between immune subsets and OS (top) or PFS (bottom) in the IHC cohort. (B) Kaplan-Meier curves for CD155 as the only IHC checkpoint significantly associated with survival, showing adverse OS in both TS (left) and TE (right). (C) Kaplan-Meier OS curves for *PVR* (CD155) in the TCGA cohort. (D) Mean gene expression of *TIGIT* and *CD226* in TCGA cervical tumors versus GTEx normal cervix. (E) Heatmaps (left) and Tukey boxplots (right) of gene signature scores across low, mid, and high *PVR* tertiles for chemotherapy resistance (top) and immunotherapy response (bottom). (F) ROC curves assessing the prognostic performance of accumulated (TS+TE) protein expression, highlighting CD155 as the marker with the highest AUC across all immune markers. (G) Heatmaps of mean normalized tumor cell proliferation (blue) or killing (red) in HeLa monocultures (left) or NK-92 co-cultures (right) under different therapies (n=6). (H) Time-course of normalized tumor killing across treatments (mean±SEM; n=6). Significance versus isotype (y=1) is shown alongside curves; significance versus aCD155 is shown in the legend. Tumor killing was derived from red object counts, normalized per treatment to the 0 hours baseline (Panel G, left), then to the corresponding monoculture (Panel G, right), and finally to the corresponding isotype (Panel H). (I) Schematic of proposed immunotype-tailored CD155-directed strategies in cervical cancer, created using BioRender. Two-tailed significance was assessed using log-rank (survival), Mann-Whitney U (tumor vs normal), Kruskal-Wallis with Dunn-Bonferroni (signature scores), and linear mixed-effects models with treatment, time point, and their interaction as fixed effects, and biological replicate as a random effect (co-cultures), all with Benjamini-Hochberg correction. Co-culture comparisons vs isotype used baseline-corrected and monoculture-corrected data; aCD155 comparisons were further isotype-corrected and assessed with Dunnett's post hoc test. Significance levels: *p<0.05, **p<0.01, ***p<0.001, and ****p<0.0001. aCD155, anti-CD155 therapy; ADC, antibody-drug conjugate; AUC, area under the curve; BiTE, bispecific T-cell engager; CAR, chimeric antigen receptor; h, hours; ICB, immune checkpoint blockade; ns, non-significant; OS, overall survival; PFS, progression-free survival; ROC, receiver operating characteristic; RSEM, RNA-Sequencing by Expectation Maximization; TE, tumor epithelium; TPM, transcripts per million; TS, tumor stroma.

no differential expression (figure 6D and online supplemental figure 6D). Prognostic analysis demonstrated favorable associations with OS for all CD155-interacting receptors, consistent with a CD155 ligand-dominant prognostic pattern (online supplemental figure 6E). Although *PVR* expression was not associated with immunotherapy response, it was progressively linked to elevated chemotherapy resistance, suggesting that CD155 may contribute to treatment-relevant tumor biology not captured by current immunotherapy response frameworks (figure 6E). Additionally, CD155 (*PVR*) consistently demonstrated the highest area under the curve (AUC) in receiver operating characteristics analyses across all markers in both cohorts (figure 6F and online supplemental figure 6F,G). Despite modest discriminative power (AUC <0.7), consistent cross-platform performance supports its potential as a biomarker and therapeutic target in cervical cancer warranting further investigation.

Together, these findings position CD155 as a robust prognostically relevant immune marker in cervical cancer.

CD155 blockade yields superior tumor cell killing compared with other clinically relevant immune checkpoint therapies

Building on CD155's consistent prognostic relevance and spatial localization, we next evaluated its functional impact in live-cell imaging-based tumor killing assays using mKate2-labeled HeLa cervical cancer cells co-cultured with NK-92 cells, treated either with CD155-targeted therapy or monotherapies targeting other major immune checkpoint axes identified in our IHC and TCGA profiling (figure 6G–H). CD155 blockade resulted in the highest level of tumor cell killing, significantly outperforming all other conditions tested, including tiragolumab (anti-TIGIT), enoblituzumab (anti-CD276), magrolimab (anti-CD47), cusatuzumab (anti-CD70), oleclumab (anti-CD73), cobolimab (anti-TIM-3), monalizumab (anti-NKG2A), and pembrolizumab (anti-PD-1). These findings offer functional support for the immunosuppressive role of CD155 and reinforce its therapeutic potential in cervical cancer. Notably, tiragolumab, enoblituzumab, and magrolimab were the only other treatments to show notable efficacy, closely aligning with the most promising targets identified in our IHC and TCGA analyses. This concordance between functional and spatial profiling data underscores the robustness of our integrative approach and highlights CD155 as a top candidate for therapeutic targeting.

DISCUSSION

Our integrative spatial and transcriptomic analysis reveals a distinct, immunotype-specific and niche-specific immune architecture in cervical cancer. Leveraging a dual-cohort design combining IHC and TCGA data, we systematically evaluated immune subsets and checkpoints, uncovering limited PD-L1 expression and highlighting alternative pathways of immune regulation. Among these, epithelial CD155 emerged as the most consistently expressed immune checkpoint and a strong prognostic and functional marker, supporting its potential as a spatially defined, therapeutic target in cervical cancer.

We first established comparability of our IHC and TCGA cohorts by benchmarking key clinicopathological characteristics against each other and national population-level data. This enabled integrative, cross-platform analyses and allowed for robust evaluation of the consistency of findings.[25] While this approach offers a comprehensive and multidimensional characterization of the cervical cancer immune landscape, some limitations warrant consideration. The exploratory design and relatively modest sample size of the IHC study limited statistical power, particularly for subgroup analyses and multiple testing correction. Additionally, the low number of progression and survival events further constrained sensitivity in survival analyses. Future dedicated studies incorporating protein-level comparison with healthy and HPV-stratified non-malignant cervical tissue, together with the transcriptomic tumor-versus-normal analyses already presented here, refined histotype-specific validation, and more physiologically representative functional models will further strengthen the biological and translational interpretation of findings like ours. Nonetheless, while these limitations may have obscured certain associations, the reproducibility of key findings across independent platforms and cohorts supports their robustness and translational relevance.

Building on this validated framework, we comprehensively profiled the spatial architecture and immunoregulatory complexity of the cervical cancer microenvironment. Unlike prior spatial protein-level studies in cervical cancer that were typically limited to few canonical markers, we assessed a broader panel encompassing both innate and adaptive immunity, enabling detailed comparison of niche-specific expression patterns. While bulk RNA-sequencing has been widely used for immune profiling in cervical cancer, it lacks spatial resolution. Emerging spatial transcriptomics in cervical cancer may address this, but its protein-level translational applicability remains limited to date.[26 27]

Leveraging this spatial resolution, we observed predominant TS localization of immune cells, with $CD8^+$ and $CD4^+$ cells being the most abundant, consistent with prior reports in cervical cancer indicating increased immune infiltration with disease progression, yet largely restricted to the TS.[28–32] While all patients in our cohorts were treatment-naïve for cervical cancer at sampling, neoadjuvant chemotherapy can alter these patterns by increasing tumor-infiltrating lymphocyte densities in cervical cancer.[33 34] $CD68^+$ cells, although more prevalent in the TS, showed the highest TE-to-TS ratio, suggesting selective enrichment in the TE. This aligns with reports of macrophage migration to the epithelial interface in cervical cancer, a phenomenon linked to HPV-mediated immune modulation.[35–37] $NKp46^+$ cells were rare, as documented in cervical cancer.[38 39] However, compared across

malignancies, cervical cancer exhibits relatively high NK cell abundance.[40] While NKp46 is a highly specific and preferred NK cell marker over CD56, its activation-dependent expression level may underestimate true NK cell prevalence.[41] NK cell exclusion correlated with poor immunotherapy response in melanoma, while infiltration predicted benefit.[42] These findings underscore that not just the presence, but the spatial positioning of immune cells may be critical for clinical response.

In addition to immune subset profiling, we assessed immune checkpoint expression to identify rational targets beyond the PD-L1/PD-1 axis in cervical cancer. HLA-E and CD47 were the most abundantly expressed immune regulators across both tumor niches, consistent with limited prior studies in cervical cancer that reported their high expression levels.[43–45] These molecules mediate non-redundant immunosuppressive functions via NKG2A/CD94 and SIRPα, respectively.[46 47] However, *HLA-E* was also abundantly expressed in normal cervical tissue, showing no tumor-specific upregulation, suggesting a role in tissue homeostasis and limiting its suitability as a selective immunotherapeutic target. In contrast, CD47, the "don't-eat-me" signal for phagocytes, was upregulated in tumor tissue compared with normal cervical epithelium. Its co-occurrence with $CD68^+$ cell enrichment in the TE suggests a macrophage-rich yet functionally suppressed tumor microenvironment. Early trials of CD47 inhibitors in solid tumors, including antibodies and fusion proteins, showed promise in several cancer types, with late-stage trials currently ongoing.[48–51] These findings advocate for the investigation of CD47-targeted strategies in cervical cancer. Notably, PD-L1 showed low expression in the IHC cohort and was the least expressed checkpoint marker in the TCGA cohort, despite being the sole approved biomarker for immune checkpoint blockade in cervical cancer.[7] This underscores growing concerns about PD-L1's predictive value and highlights the utility of broader checkpoint profiling.[6 52 53] LAG-3, the only receptor in our panel due to its context-dependent and poorly defined ligands, showed low expression, consistent with prior reports in cervical cancer and its transient nature compared with more stable ligand expression.[54–56] Interestingly, pan-cancer analyses rank cervical tumors among the highest LAG-3 expressers.[55] Despite its low abundance, LAG-3 correlated strongly with CD8 and CD4 markers, consistent with its role in T-cell exhaustion and activation-dependent dynamics.[55 57] We further identified tumor niche-specific expression patterns, including TE enrichment of CD276 and CD155, and TS enrichment of CD70 and CD73. Although direct spatial data for CD276, CD70, and CD73 in cervical cancer is lacking, one prior study similarly reported tumorous enrichment of CD155, though lacked tumor niche distinction.[58] Overall, niche-specific checkpoint patterns may inform spatially tailored immunotherapy combinations.

Clinicopathological profiling revealed distinct immune landscapes across cervical cancer histotypes. SCC demonstrated higher immune infiltration and checkpoint expression than AC, aligning with TCGA classifications and likely driven by molecular features such as PI3K/AKT signaling and APOBEC activity.[9] Prior studies support our findings, reporting higher tumor mutational burden, PD-L1 expression, and immune infiltration in cervical SCC.[59–61] Beyond PD-L1, histotype-specific checkpoint expression remains largely unexplored. One IHC study compared Gal-9 between histotypes and confirmed higher expression in cervical SCC.[62] Another found elevated HLA-E expression in cervical AC compared with SCC, contrasting our data.[45] These limited available data underscore the value of our study in advancing histotype-specific characterization of alternative checkpoint expression in cervical cancer. Although the AC subgroup in the IHC cohort was relatively small, the use of non-parametric testing with false discovery rate correction, together with independent validation in the larger TCGA cohort, supports the robustness of the histotype-associated differences we observed. Nonetheless, further dedicated studies are warranted to refine histotype-guided therapeutic strategies.

As tumor immunotypes are emerging as key determinants of immunotherapy response, we next stratified tumors by spatial $CD8^+$-defined immunotypes, revealing distinct biological and clinical features in cervical cancer. Immune-inflamed tumors predominated in our cohort and exhibited higher immune subset and checkpoint expression, whereas immune-desert tumors showed minimal infiltration and poorer outcomes, consistent with their established resistance to checkpoint blockade.[21–24] The relatively low frequency of immune-desert tumors in our cohort may reflect true biological rarity or selection bias in our cohort toward earlier-stage, more immune-active disease. Unlike transcriptomic frameworks, our study provides spatially resolved protein-level data, uncovering niche-specific immune patterns linked to immunotypes. Previous studies have consistently associated immune-rich cervical cancers with increased T cell infiltration and PD-L1 expression.[63–66] Only one extended this analysis to include HLA-E, reporting its upregulation in immune-infiltrated tumors.[66] We expand these findings by mapping a broader panel of immune markers across tumor niches and linking them to tumor immunotypes, thereby offering novel translational insights not captured by transcriptomic data alone. All immune markers showed stepwise increased expression from immune-desert to immune-inflamed tumors. Intriguingly, TE expression of CD155 was highest in immune-desert tumors and the only marker elevated in this phenotype. Beyond immune evasion, CD155 also regulates proliferation, adhesion, migration and invasion.[67] These observations warrant further research to dissect immunoregulatory and tumor-intrinsic roles of distinct and shared checkpoints across immunotypes in cervical cancer.

Survival analyses identified prognostic relevance of specific immune markers. CD8, CD4, CD4-FoxP3, and NKp46 were significantly associated with improved survival in both IHC and TCGA cohorts. Our IHC data

demonstrated that this effect was niche-dependent, with CD4, CD4-FoxP3, and NKp46 in TS and CD8 in TE, the latter supporting prior studies in cervical cancer.[35 68] Among immune checkpoint markers, CD155 emerged as the only consistent adverse prognostic indicator, with elevated expression linked to chemotherapy resistance and worse outcomes across both tumor niches, patient cohorts and data platforms. This supports its immunosuppressive function within the TIGIT axis, recognized for dampening the T and NK cell activity in cervical cancer.[56 58 69 70] However, *PVR* showed no association with immunotherapy response in our study. Moreover, clinical trials of TIGIT blockade in cervical cancer—SKYSCRAPER-04, KEYVIBE-005, and AdvanTIG-202—have shown only modest response improvements without statistically significant survival benefit over anti-PD-1 monotherapy.[71–73] These findings mirror results of anti-TIGIT trials in other cancer types and suggest that this receptor-based approach may not fully exploit the therapeutic potential of the CD155/TIGIT axis.[74] Indeed, our functional assays showed that direct CD155 blockade induced superior tumor cell killing than anti-TIGIT or other checkpoint therapies. Although performed in HeLa cells, an AC-derived model despite SCC predominating in our cohorts, these proof-of-principle findings align with emerging translational and clinical evidence that CD155-targeted therapies enhance NK cell-mediated killing and can outperform TIGIT inhibition in solid tumor models.[75–77]

Our spatial profiling revealed that CD155 is consistently and highly enriched in the TE across all immunotypes, including immune-desert tumors where few other immune markers are present, indicative of additional non-immunological, tumor-intrinsic functions.[67] Its minimal TS expression positions CD155 as a compelling and underused therapeutic target in cervical cancer. Rather than solely acting through checkpoint inhibition, this epithelial specificity supports exploring CD155-directed approaches that align with its spatial distribution. Based on our study, we propose immunotype-tailored, epithelial-targeted modalities directed against CD155 (figure 6I). In immune-inflamed tumors, approaches such as blocking antibodies, bispecific T cell engagers (BiTEs), or engineered cell therapies may be particularly effective. NTX1088, a first-in-class anti-CD155 monoclonal antibody, is currently in phase I trials alone and with pembrolizumab for advanced solid tumors.[75] Preliminary biomarker analyses demonstrate restoration of DNAM-1 on immune cells, marking the first evidence of DNAM-1 upregulation in a clinical setting and suggesting renewed sensitivity to immunotherapy.[78] BiTEs targeting CD155 offer an additional therapeutic strategy. CD155xCD3 constructs significantly enhanced cytotoxicity against $CD155^{+}$ cancer cells and promoted T cell activation, cytokine release, and expression of cytolytic mediators in several preclinical models, including cervical cancer.[79] Chimeric antigen receptor (CAR) therapy has revolutionized oncology in recent years. While CAR-T cells act independently of pre-existing lymphocytes, their efficacy is influenced by the tumor microenvironment, particularly their ability to infiltrate and persist.[80] In line with our findings, recent pan-cancer analyses support CD155 as a promising CAR-T target.[77] Indeed, CD155-targeting CAR-T cells demonstrated potent preclinical efficacy across various tumor models with favorable safety profiles, including in cervical cancer.[77 81–83] In immune-desert or immune-excluded tumors, however, these approaches might be insufficient on their own due to the lack of immune infiltrate. Instead, antibody-drug conjugates (ADCs) and oncolytic viruses offer alternatives by directly killing tumor cells and priming the microenvironment. Tisotumab-vedotin, recently approved for recurrent or metastatic cervical cancer, exemplifies the clinical viability of ADCs for these patients, allowing tumor-specific delivery of high-dose cytotoxic therapy.[84] CD155-targeted ADCs are supported by evidence of CD155 internalization, a mechanistic prerequisite, while a first-in-class CD155-ADC is expected to enter investigational new drug-enabling studies this year.[85] Among oncolytic viruses, PVSRIPO, a non-neurovirulent rhinovirus:poliovirus chimera with natural CD155 tropism, has shown immune engagement and antitumor effects in mouse models and early clinical promise in melanoma and glioblastoma.[86–88] Collectively, we advocate for a paradigm shift regarding the therapeutic application of the TIGIT axis, repositioning CD155 from a passive immune checkpoint to an active target for precision immunotherapy tailored to tumor architecture and immune contexture. Future mechanistic studies using advanced patient-derived and in vivo model systems will be critical to validate this therapeutic potential in cervical cancer.

In conclusion, our integrative spatial and transcriptomic profiling uncovers a complex, niche-specific and immunotype-specific immune landscape in cervical cancer that extends beyond the PD-L1/PD-1 axis and includes targets with actionable drug coverage. Among these, CD155 emerged as the strongest prognostic marker, consistently enriched in the TE across all immunotypes, including immune-desert tumors. While CD155 blockade most effectively restored antitumor immunity, its reliance on immune effector cells may limit efficacy in immune-cold tumors, underscoring the need to move beyond classical checkpoint strategies in such settings. In this context, CD155's consistent and near-exclusive epithelial expression positions it as a uniquely actionable target for both checkpoint inhibition and epithelial-directed, spatially informed precision therapies in cervical cancer.

Author affiliations
[1]Center for Oncological Research (CORE), University of Antwerp, Antwerp, Flanders, Belgium
[2]Multidisciplinary Oncology Center Antwerp (MOCA), Antwerp University Hospital, Edegem, Flanders, Belgium
[3]Data Science Institute, I-Biostat, Hasselt University, Hasselt, Flanders, Belgium
[4]Department of Pathology, PA², General Hospital ZAS Middelheim, Antwerp, Flanders, Belgium
[5]Department of Pathology, University Hospital Antwerp, Edegem, Flanders, Belgium

[6]Department of Gynaecology, General Hospital ZAS Augustine, Wilrijk, Flanders, Belgium
[7]Multidisciplinary Breast Cancer and Gynaecologic Oncology Unit, University Hospital Antwerp, Edegem, Flanders, Belgium

Acknowledgements The authors wish to thank the histopathology and biobank teams at UZA and ZAS Hospital for their support in providing tumor specimens and assisting with sample processing. We also acknowledge the TCGA Research Network, GTEx Project, and the Belgian Cancer Registry for making their data publicly available. We extend our sincere gratitude to the funding agencies whose support was instrumental in enabling this research.

Contributors All authors contributed to the study as follows: conceptualization, study design, and supervision (YV, SK, PAvD, JDW); experiments (YV, HL, CH, KZ, HS); data analysis and interpretation (YV, DQ, SvdH, JC, JDB, GB, HVD, AR, HS, SVL, CF, LCvK, SK, PAvD, JDW); data collection/curation (YV, JH, PAvD); original draft preparation (YV, JDW); and manuscript review, editing, and approval (all authors). JDW is the guarantor of the study. Artificial intelligence (AI) tools, including ChatGPT (OpenAI), were used to support manuscript text editing and to assist with code writing for data analysis and figure generation.

Funding This study was supported by research grants from Kom op tegen Kanker (Stand up to Cancer), the Flemish cancer society, and the Multidisciplinary Oncology Center Antwerp (MOCA) from the Antwerp University Hospital. YV (1S69721N) and DQ (1S76421N) were PhD fellows of the Research Foundation Flanders (FWO). YV also received support from the Emmanuel van der Schueren research grant (CS 16628) of Kom op tegen Kanker. We are also grateful for donations from individual patrons, including Reynaers Aluminium NV, Dedert Schilde vzw, Willy Floren and the Vereycken family. The funders had no role in study design, in the collection, analysis or interpretation of data, in the writing of the report, or in the decision to submit the article for publication. They did not influence the results or conclusions of the study.

Competing interests GB participated in the advisory boards for Roche, AstraZeneca, and MSD. GB is/was a consultant for AstraZeneca, MSD, Novartis and Roche. GB has no financial conflicts of interest related to the current work presented.

Patient consent for publication Not applicable.

Provenance and peer review Not commissioned; externally peer reviewed.

Data availability statement Data are available upon reasonable request. De-identified participant data from the IHC cohort, along with supporting materials, are available from the corresponding author upon reasonable request, subject to institutional and ethical approvals. TCGA data are publicly available through the National Cancer Institute Genomic Data Commons and accessible via platforms such as cBioPortal.

ORCID iD
Yannick Verhoeven https://orcid.org/0000-0002-4168-8222

REFERENCES

1 Ferlay J, Ervik M, Lam F, *et al*. Global cancer observatory: cancer today. lyon, france: international agency for research on cancer. 2024. Available: https://gco.iarc.who.int/today
2 Lo Cigno I, Calati F, Girone C, *et al*. High-risk HPV oncoproteins E6 and E7 and their interplay with the innate immune response: Uncovering mechanisms of immune evasion and therapeutic prospects. *J Med Virol* 2024;96:e29685.
3 Alexandrov LB, Nik-Zainal S, Wedge DC, *et al*. Signatures of mutational processes in human cancer. *Nature New Biol* 2013;500:415–21.
4 Mandal R, Şenbabaoğlu Y, Desrichard A, *et al*. The head and neck cancer immune landscape and its immunotherapeutic implications. *JCI Insight* 2016;1:e89829.
5 Chung HC, Ros W, Delord J-P, *et al*. Efficacy and Safety of Pembrolizumab in Previously Treated Advanced Cervical Cancer: Results From the Phase II KEYNOTE-158 Study. *JCO* 2019;37:1470–8.
6 Verhoeven Y, Quatannens D, Trinh XB, *et al*. Targeting the PD-1 Axis with Pembrolizumab for Recurrent or Metastatic Cancer of the Uterine Cervix: A Brief Update. *Int J Mol Sci* 2021;22:1807.
7 Colombo N, Dubot C, Lorusso D, *et al*. Pembrolizumab for Persistent, Recurrent, or Metastatic Cervical Cancer. *N Engl J Med* 2021;385:1856–67.
8 Tiwari A, Oravecz T, Dillon LA, *et al*. Towards a consensus definition of immune exclusion in cancer. *Front Immunol* 2023;14:1084887.
9 The Cancer Genome Atlas Research Network. Integrated genomic and molecular characterization of cervical cancer. *Nature New Biol* 2017;543:378–84.
10 Cerami E, Gao J, Dogrusoz U, *et al*. The cBio cancer genomics portal: an open platform for exploring multidimensional cancer genomics data. *Cancer Discov* 2012;2:401–4.
11 Wang X, Chen L, Liu W, *et al*. TIMEDB: tumor immune micro-environment cell composition database with automatic analysis and interactive visualization. *Nucleic Acids Res* 2023;51:D1417–24.
12 Lonsdale J, Thomas J, Salvatore M, *et al*. The Genotype-Tissue Expression (GTEx) project. *Nat Genet* 2013;45:580–5.
13 Fang J, Wang Y, Li C, *et al*. A hypoxia-derived gene signature to suggest cisplatin-based therapeutic responses in patients with cervical cancer. *Comput Struct Biotechnol J* 2024;23:2565–79.
14 Olaussen KA, Dunant A, Fouret P, *et al*. DNA repair by ERCC1 in non-small-cell lung cancer and cisplatin-based adjuvant chemotherapy. *N Engl J Med* 2006;355:983–91.
15 Aldonza MBD, Hong J-Y, Alinsug MV, *et al*. Multiplicity of acquired cross-resistance in paclitaxel-resistant cancer cells is associated with feedback control of TUBB3 via FOXO3a-mediated ABCB1 regulation. *Oncotarget* 2016;7:34395–419.
16 Ayers M, Lunceford J, Nebozhyn M, *et al*. IFN-γ-related mRNA profile predicts clinical response to PD-1 blockade. *J Clin Invest* 2017;127:2930–40.
17 Hugo W, Zaretsky JM, Sun L, *et al*. Genomic and Transcriptomic Features of Response to Anti-PD-1 Therapy in Metastatic Melanoma. *Cell* 2016;165:35–44.
18 Van den Eynde A, Gehrcken L, Verhezen T, *et al*. IL-15-secreting CAR natural killer cells directed toward the pan-cancer target CD70 eliminate both cancer cells and cancer-associated fibroblasts. *J Hematol Oncol* 2024;17:8.
19 Deben C, De La Hoz EC, Compte ML, *et al*. OrBITS: label-free and time-lapse monitoring of patient derived organoids for advanced drug screening. *Cell Oncol (Dordr)* 2023;46:299–314.
20 Camp RL, Dolled-Filhart M, Rimm DL. X-tile: a new bio-informatics tool for biomarker assessment and outcome-based cut-point optimization. *Clin Cancer Res* 2004;10:7252–9.
21 Chen DS, Mellman I. Elements of cancer immunity and the cancer–immune set point. *Nature New Biol* 2017;541:321–30.
22 de Biase D, Lenzi J, Ceccarelli C, *et al*. Spatial Cancer-Immune Phenotypes Predict Shorter Recurrence-Free Survival in the No Specific Molecular Profile Molecular Subtype of Endometrial Carcinoma. *Mod Pathol* 2025;38:100624.
23 Herbst RS, Soria J-C, Kowanetz M, *et al*. Predictive correlates of response to the anti-PD-L1 antibody MPDL3280A in cancer patients. *Nature New Biol* 2014;515:563–7.
24 Mellman I, Chen DS, Powles T, *et al*. The cancer-immunity cycle: Indication, genotype, and immunotype. *Immunity* 2023;56:2188–205.
25 Okamoto J, Yin X, Ryan B, *et al*. Multi-INTACT: integrative analysis of the genome, transcriptome, and proteome identifies causal mechanisms of complex traits. *Genome Biol* 2025;26:19.
26 Fan J, Lu F, Qin T, *et al*. Multiomic analysis of cervical squamous cell carcinoma identifies cellular ecosystems with biological and clinical relevance. *Nat Genet* 2023;55:2175–88.
27 Zhou L, Liu J, Yao P, *et al*. Spatial transcriptomics reveals unique metabolic profile and key oncogenic regulators of cervical squamous cell carcinoma. *J Transl Med* 2024;22:1163.
28 Litwin TR, Irvin SR, Chornock RL, *et al*. Infiltrating T-cell markers in cervical carcinogenesis: a systematic review and meta-analysis. *Br J Cancer* 2021;124:831–41.

29 Zhang J, Meng S, Zhang X, *et al*. Infiltration Patterns of Cervical Epithelial Microenvironment Cells During Carcinogenesis. *Front Immunol* 2022;13:888176.
30 Chen R, Gong Y, Zou D, *et al*. Correlation between subsets of tumor-infiltrating immune cells and risk stratification in patients with cervical cancer. *PeerJ* 2019;7:e7804.
31 Bedoya AM, Jaramillo R, Baena A, *et al*. Location and Density of Immune Cells in Precursor Lesions and Cervical Cancer. *Cancer Microenviron* 2013;6:69–77.
32 Ring KL, Yemelyanova AV, Soliman PT, *et al*. Potential immunotherapy targets in recurrent cervical cancer. *Gynecol Oncol* 2017;145:462–8.
33 Heeren AM, van Luijk IF, Lakeman J, *et al*. Neoadjuvant cisplatin and paclitaxel modulate tumor-infiltrating T cells in patients with cervical cancer. *Cancer Immunol Immunother* 2019;68:1759–67.
34 Zhang Y, Yu M, Jing Y, *et al*. Baseline immunity and impact of chemotherapy on immune microenvironment in cervical cancer. *Br J Cancer* 2021;124:414–24.
35 Dimitrova P, Vasileva-Slaveva M, Shivarov V, *et al*. Infiltration by Intratumor and Stromal CD8 and CD68 in Cervical Cancer. *Medicina (Kaunas)* 2023;59:728.
36 Raonic J, Lopicic M, Vuckovic L, *et al*. Immunohistochemical analysis of CD68, CD4, CD8 and CD20 expression in cervical dysplasia and its relationship with HR-HPV infection. *Eur Rev Med Pharmacol Sci* 2021;25:27458:7598–606:.
37 de Vos van Steenwijk PJ, Ramwadhdoebe TH, Goedemans R, *et al*. Tumor-infiltrating CD14-positive myeloid cells and CD8-positive T-cells prolong survival in patients with cervical carcinoma. *Intl Journal of Cancer* 2013;133:2884–94.
38 Garcia-Iglesias T, Del Toro-Arreola A, Albarran-Somoza B, *et al*. Low NKp30, NKp46 and NKG2D expression and reduced cytotoxic activity on NK cells in cervical cancer and precursor lesions. *BMC Cancer* 2009;9:186.
39 Gutiérrez-Hoya A, Soto-Cruz I. NK Cell Regulation in Cervical Cancer and Strategies for Immunotherapy. *Cells* 2021;10:3104.
40 Cózar B, Greppi M, Carpentier S, *et al*. Tumor-Infiltrating Natural Killer Cells. *Cancer Discov* 2021;11:34–44.
41 Ma R, Li Z, Tang H, *et al*. NKp46 enhances type 1 innate lymphoid cell proliferation and function and anti-acute myeloid leukemia activity. *Nat Commun* 2025;16:989.
42 Pozniak J, Roda N, Landeloos E, *et al*. Cytotoxic NK Cells Impede Response to Checkpoint Immunotherapy in Melanoma with an Immune-Excluded Phenotype. *Cancer Discov* 2025;15:1819–34.
43 Gooden M, Lampen M, Jordanova ES, *et al*. HLA-E expression by gynecological cancers restrains tumor-infiltrating CD8+T lymphocytes.. *Proc Natl Acad Sci U S A* 2011;108:10656–61.
44 Yordanov A, Shivarov V, Kostov S, *et al*. Prognostic Utility of CD47 in Cancer of the Uterine Cervix and the Sensitivity of Immunohistochemical Scores. *Diagnostics (Basel)* 2022;13:52.
45 Spaans VM, Peters AAW, Fleuren GJ, *et al*. HLA-E expression in cervical adenocarcinomas: association with improved long-term survival. *J Transl Med* 2012;10:184.
46 Li Y, Li Z, Tang Y, *et al*. Unlocking the therapeutic potential of the NKG2A-HLA-E immune checkpoint pathway in T cells and NK cells for cancer immunotherapy. *J Immunother Cancer* 2024;12:e009934.
47 Liu Y, Weng L, Wang Y, *et al*. Deciphering the role of CD47 in cancer immunotherapy. *J Adv Res* 2024;63:129–58.
48 Lakhani NJ, Chow LQM, Gainor JF, *et al*. Evorpacept alone and in combination with pembrolizumab or trastuzumab in patients with advanced solid tumours (ASPEN-01): a first-in-human, open-label, multicentre, phase 1 dose-escalation and dose-expansion study. *Lancet Oncol* 2021;22:1740–51.
49 Eng C, Lakhani NJ, Philip PA, *et al*. A Phase 1b/2 Study of the Anti-CD47 Antibody Magrolimab with Cetuximab in Patients with Colorectal Cancer and Other Solid Tumors. *Target Oncol* 2025;20:519–30.
50 Lakhani NJ, Stewart D, Richardson DL, *et al*. First-in-human phase I trial of the bispecific CD47 inhibitor and CD40 agonist Fc-fusion protein, SL-172154 in patients with platinum-resistant ovarian cancer. *J Immunother Cancer* 2025;13:e010565.
51 Yang J, Song Y, Zhou K, *et al*. Safety and efficacy of amulirafusp alfa (IMM0306), a fusion protein of CD20 monoclonal antibody with the CD47 binding domain of SIRPα, in patients with relapsed or refractory B-cell non-Hodgkin lymphoma: a phase 1/2 study. *J Hematol Oncol* 2024;17:123.
52 Wang N, Nanding A, Jia X, *et al*. Mining of immunological and prognostic-related biomarker for cervical cancer based on immune cell signatures. *Front Immunol* 2022;13:993118.
53 Rotman J, den Otter LAS, Bleeker MCG, *et al*. PD-L1 and PD-L2 Expression in Cervical Cancer: Regulation and Biomarker Potential. *Front Immunol* 2020;11:596825.
54 Hirahara Y, Shimizu K, Yamasaki S, *et al*. Crucial immunological roles of the invasion front in innate and adaptive immunity in cervical cancer. *Br J Cancer* 2024;131:1762–74.
55 Panda A, Rosenfeld JA, Singer EA, *et al*. Genomic and immunologic correlates of LAG-3 expression in cancer. *Oncoimmunology* 2020;9:1756116.
56 Zou W, Huang R, Li P, *et al*. Clinical significance of immune checkpoint proteins in HPV-infected cervical cancer. *J Infect Public Health* 2023;16:542–50.
57 Ngiow SF, Manne S, Huang YJ, *et al*. LAG-3 sustains TOX expression and regulates the CD94/NKG2-Qa-1b axis to govern exhausted CD8 T cell NK receptor expression and cytotoxicity. *Cell* 2024;187:4336–54.
58 Wang Y, Wang C, Qiu J, *et al*. Targeting CD96 overcomes PD-1 blockade resistance by enhancing CD8+ TIL function in cervical cancer. *J Immunother Cancer* 2022;10:e003667.
59 Heeren AM, Punt S, Bleeker MC, *et al*. Prognostic effect of different PD-L1 expression patterns in squamous cell carcinoma and adenocarcinoma of the cervix. *Mod Pathol* 2016;29:753–63.
60 Huang RSP, Haberberger J, Murugesan K, *et al*. Clinicopathologic and genomic characterization of PD-L1-positive uterine cervical carcinoma. *Mod Pathol* 2021;34:1425–33.
61 Li J, Xue X, Zhang Y, *et al*. The differences in immune features and genomic profiling between squamous cell carcinoma and adenocarcinoma - A multi-center study in Chinese patients with uterine cervical cancer. *Gynecol Oncol* 2023;175:133–41.
62 Beyer S, Wehrmann M, Meister S, *et al*. Galectin-8 and -9 as prognostic factors for cervical cancer. *Arch Gynecol Obstet* 2022;306:1211–20.
63 Ghosh A, Ghosh A, Sinha A, *et al*. Identification of HPV16 positive cervical cancer subsets characterized by divergent immune and oncogenic phenotypes with potential implications for immunotherapy. *Tumour Biol* 2023;45:55–69.
64 Li Y, Lu S, Wang S, *et al*. Identification of immune subtypes of cervical squamous cell carcinoma predicting prognosis and immunotherapy responses. *J Transl Med* 2021;19:222.
65 Lyu X, Li G, Qiao Q. Identification of an immune classification for cervical cancer and integrative analysis of multiomics data. *J Transl Med* 2021;19:200.
66 Song G, Luo J, Zou S, *et al*. Molecular classification of human papillomavirus-positive cervical cancers based on immune signature enrichment. *Front Public Health* 2022;10:979933.
67 O'Donnell JS, Madore J, Li X-Y, *et al*. Tumor intrinsic and extrinsic immune functions of CD155. *Semin Cancer Biol* 2020;65:189–96.
68 Piersma SJ, Jordanova ES, van Poelgeest MIE, *et al*. High number of intraepithelial CD8+ tumor-infiltrating lymphocytes is associated with the absence of lymph node metastases in patients with large early-stage cervical cancer. *Cancer Res* 2007;67:354–61.
69 Liu L, Wang A, Liu X, *et al*. Blocking TIGIT/CD155 signalling reverses $CD8^+$ T cell exhaustion and enhances the antitumor activity in cervical cancer. *J Transl Med* 2022;20:280.
70 Liu L, Wang Y, Geng C, *et al*. CD155 Promotes the Progression of Cervical Cancer Cells Through AKT/mTOR and NF-κB Pathways. *Front Oncol* 2021;11:655302.
71 Leary A, Yonemori K, Le Tourneau C, *et al*. 21O Coformulated vibostolimab/pembrolizumab in advanced cervical cancer: KEYVIBE-005. *ESMO Open* 2024;9:103521.
72 Salani R, McCormack M, Kim Y-M, *et al*. A non-comparative, randomized, phase II trial of atezolizumab or atezolizumab plus tiragolumab for programmed death-ligand 1-positive recurrent cervical cancer (SKYSCRAPER-04). *Int J Gynecol Cancer* 2024;34:1140–8.
73 Lee J-Y, Boonyapipat S, Yuan G, *et al*. AdvanTIG-202: Phase 2 open-label, two-cohort multicenter study of ociperlimab plus tislelizumab and tislelizumab alone in patients with previously treated recurrent or metastatic cervical cancer. *Gynecol Oncol* 2025;198:25–32.
74 Rousseau A, Parisi C, Barlesi F. Anti-TIGIT therapies for solid tumors: a systematic review. *ESMO Open* 2023;8:101184.
75 Atieh A, Obeidat A, Vitenshtein A, *et al*. Abstract 7539: First-in-class anti-PVR mAb NTX1088 advancing through Phase I: Safe and potent in restoring DNAM1 expression to enhance antitumor immunity. *Cancer Res* 2024;84:7539.
76 Cho MM, Song L, Quamine AE, *et al*. CD155 blockade enhances allogeneic natural killer cell-mediated antitumor response against osteosarcoma. *J Immunother Cancer* 2025;13:e008755.
77 Liu X, Sun Y, Lin B, *et al*. Pan-cancer analysis identifies CD155 as a promising target for CAR-T cell therapy. *Genome Med* 2025;17:64.
78 Braun M, Aguilera AR, Sundarrajan A, *et al*. CD155 on Tumor Cells Drives Resistance to Immunotherapy by Inducing the Degradation of the Activating Receptor CD226 in $CD8^+$ T Cells. *Immunity* 2020;53:805–23.

79 Ma L, Ma J, Feng D, *et al*. Bispecific antibody targeting CD155 mediates T-cell immunotherapy against human gynecological malignancies. *Invest New Drugs* 2025;43:318–27.
80 Liu Z, Zhou Z, Dang Q, *et al*. Immunosuppression in tumor immune microenvironment and its optimization from CAR-T cell therapy. *Theranostics* 2022;12:6273–90.
81 Xiong T, Wang G, Yu P, *et al*. CAR-T cells targeting CD155 reduce tumor burden in preclinical models of leukemia and solid tumors. *J Clin Invest* 2025;135:e189920.
82 Zhang K, Mi Y, Zhang B, *et al*. Preclinical application of a CD155 targeting chimeric antigen receptor T cell therapy for digestive system cancers. *Oncogene* 2025;44:1463–74.
83 Ma J, Zhu W, Zhao R, *et al*. CD155-based chimeric antigen receptor T cells: a promising immunotherapy for cervical and breast cancer. *Front Immunol* 2025;16:1631812.
84 Vergote I, González-Martín A, Fujiwara K, *et al*. Tisotumab Vedotin as Second- or Third-Line Therapy for Recurrent Cervical Cancer. *N Engl J Med* 2024;391:44–55.
85 Fujito T, Ikeda W, Kakunaga S, *et al*. Inhibition of cell movement and proliferation by cell–cell contact-induced interaction of Necl-5 with nectin-3. *J Cell Biol* 2005;171:165–73.
86 Mosaheb MM, Dobrikova EY, Brown MC, *et al*. Genetically stable poliovirus vectors activate dendritic cells and prime antitumor CD8 T cell immunity. *Nat Commun* 2020;11:524.
87 Beasley GM, Nair SK, Farrow NE, *et al*. Phase I trial of intratumoral PVSRIPO in patients with unresectable, treatment-refractory melanoma. *J Immunother Cancer* 2021;9:e002203.
88 Desjardins A, Gromeier M, Herndon JE II, *et al*. Recurrent Glioblastoma Treated with Recombinant Poliovirus. *N Engl J Med* 2018;379:150–61.